Liquid-Metal Droplet Coalescence in Metallurgical Slags: A Critical Review of Interfacial Phenomena, Slag Properties, Hydrodynamics, Kinetics, and Metal Recovery

Antonio Clareti Pereira*

PhD in Chemical Engineering, University of São Paulo (USP), Belo Horizonte, Minas Gerais, Brazil

***Corresponding Author: claretipereira@gmail.com**

ORCID: 0000-0001-8115-4279

DOI: https://doi.org/10.47772/IJRISS.2026.100701023

Received: 06 August 2026; Accepted: 12 August 2026; Published: 19 August 2026

ABSTRACT

Metal losses to metallurgical slags arise from fundamentally different mechanisms: chemical dissolution in the oxide or salt phase and physical entrainment of discrete liquid-metal or matte droplets. This distinction is decisive because only the physically entrained fraction can be directly targeted by collision, coalescence, settling, or forced-separation strategies. This structured critical narrative review integrates a retained contemporary corpus of 108 publications from 2020 to August 2026, supplemented by four foundational pre-2020 mechanistic sources used only to anchor classical droplet-transport, breakup, coalescence, and population-balance concepts and excluded from the corpus count. The review examines how droplet generation, interfacial chemistry, slag rheology, hydrodynamics, and residence time jointly determine whether dispersed metal is recovered or discarded with slag. The review develops a Droplet–Interface–Slag–Hydrodynamics–Recovery (D–I–S–H–R) framework and emphasizes five coupled controls: droplet-size distribution, dynamic interfacial tension and wetting, slag viscosity and solid fraction, collision-versus-breakup hydrodynamics, and the time/force available for phase separation. Evidence from copper-slag cleaning, aluminum salt-flux processing, iron-droplet assembly, steel–slag emulsification, and supergravity separation shows that lower viscosity and larger droplets generally favor separation, but the response is non-monotonic because additives and mixing can simultaneously alter liquidus temperature, interfacial reactions, droplet breakup, oxidation, refractory interaction, and metal quality. A central conclusion is that “more mixing” is not equivalent to “more recovery”: useful operation requires a finite hydrodynamic window in which collision frequency is increased without creating a finer steady-state dispersion, followed by sufficient low-turbulence or forced-separation time. The literature remains limited by scarce in-situ droplet-size measurements, dynamic high-temperature interfacial data, closed metal balances, industrial validation of multiphase models, and standardized reporting of uncertainty. The proposed framework converts these gaps into a process decision sequence for diagnosing metal loss, conditioning slag, managing interfaces, tuning mixing, and providing adequate separation before tapping.

Keywords: liquid-metal droplets; metallurgical slag; coalescence; interfacial tension; slag viscosity; metal recovery

Highlights

- Distinguishes chemically dissolved metal from physically entrained recoverable droplets.
- Integrates interfacial chemistry, slag rheology, droplet dynamics, and hydrodynamics in one framework.
- Shows that mixing has an optimum window because collision enhancement competes with breakup and redispersion.
- Proposes a D–I–S–H–R decision framework linking droplet-scale mechanisms to industrial metal recovery.

INTRODUCTION

Metal losses to metallurgical slags

Metallurgical slags are simultaneously process media, chemical sinks, heat carriers, and repositories for unrecovered metal. The economic significance of a given slag therefore cannot be inferred from total metal concentration alone. A chemically dissolved species requires a change in equilibrium, oxygen potential, activity, or reduction state before it can be recovered, whereas an entrained metallic or matte droplet is already a separate liquid phase and can be recovered by growth and physical separation. Recent work on copper, steelmaking, ferroalloy, aluminum, red-mud, and complex secondary-resource slags illustrates the breadth of this distinction and the consequence of treating "metal in slag" as a single category (Avarmaa et al., 2025; Eray et al., 2022; Klaffenbach et al., 2023; Klaffenbach et al., 2021; Li et al., 2022; Mongoljiibuu et al., 2025; Pereira, 2025a; Pereira, 2025b).

For process design, the physically entrained fraction is the direct target of coalescence engineering. Its recoverability depends on whether droplets can move relative to the slag, encounter one another, drain the intervening film, merge into larger bodies, and then traverse the slag layer before solidification or tapping. This sequence can be interrupted at every step by viscous drag, interfacial films, high solid fraction, chemical reaction, inadequate residence time, or renewed turbulence. Conversely, chemically generated droplets can appear during reduction and create a moving target in which droplet birth and separation occur simultaneously (He et al., 2020; Jing et al., 2025; Lai et al., 2026; Lin et al., 2021; Liu et al., 2026; Liu, Xu, et al., 2023; Xin et al., 2020; Xu et al., 2023; Xu, Liu, et al., 2022; Xu, Zhang, et al., 2022; L. Zhang & Chen, 2023).

Why droplet coalescence matters

Droplet size is a bridge variable between chemistry and separation. At low Reynolds number, the gravitational settling velocity scales approximately with the square of droplet diameter, so even modest coalescence can strongly increase the separation rate. Larger droplets are also less sensitive to small-scale turbulent eddies and are more likely to penetrate interfacial barriers, while very fine droplets can remain suspended long enough to be frozen into a solidifying slag. The importance of size distribution is evident in experimental and modeling studies of iron and generic liquid–liquid droplet sedimentation and in industrial copper-slag cleaning (He et al., 2020; Lai et al., 2026; Mitas et al., 2023; Qian et al., 2023; Q.-M. Wang, Huang, et al., 2023; Isaksson et al., 2023).

The entrainment–coalescence–separation problem

The useful conceptual sequence is not simply "slag cleaning → metal recovery." It is: metal generation → droplet formation → dispersion → collision → film drainage → coalescence or rebound → settling/forced separation → recovery. Breakup, oxidation, dissolution, and re-entrainment compete with this forward pathway. The literature on droplet bouncing and partial coalescence, bubble-mediated interfacial disturbance, emulsification, and interfacial reaction confirms that contact between phases cannot be equated with successful separation (Chang et al., 2021; Cheng et al., 2024; Liu, Cheng, et al., 2023; Liu et al., 2024; McGuan et al., 2022; Minami et al., 2023; Mirjalili & Chan, 2021; Park et al., 2021; Silva et al., 2021; J. Zhang et al., 2023; Zhao et al., 2022).

Figure 1 is inserted here because the review's central argument is mechanistic: industrial metal recovery is the endpoint of coupled droplet, interface, slag, hydrodynamic, and thermal/chemical controls rather than a response to one independent variable.

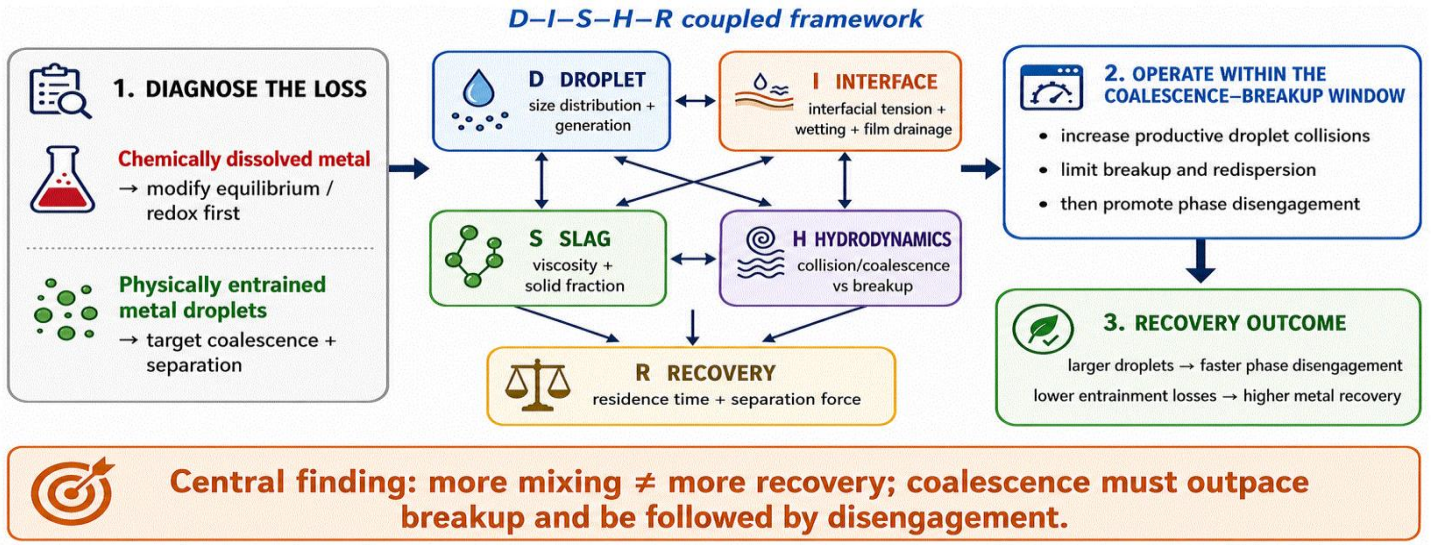

Figure 1. Integrated sequence from liquid-metal or matte droplet generation to recovered metal and the principal coupled controls.

Note. Adapted from the conceptual integration of droplet generation, coalescence, settling, wetting, rheology, and industrial recovery described by He et al. (2020), McGuan et al. (2022), Qian et al. (2023), Isaksson et al. (2023), and Lai et al. (2026).

The integrated view in Figure 1 also explains why isolated optimization can fail. A flux that decreases viscosity may accelerate settling but alter interfacial tension; stronger stirring may increase encounters but shift the droplet-size distribution toward smaller sizes; and longer holding can improve separation while increasing oxidation or energy use. The operative objective is therefore to maximize net metal recovery, not any single intermediate parameter.

Limitations of existing reviews

Recent reviews and process overviews often emphasize slag utilization, aluminum recycling, salt-flux practice, steelmaking-slag valorization, or copper-slag processing, but this literature is usually organized around feedstock, products, or process routes rather than the full droplet-scale chain. As a result, viscosity data may be discussed separately from interfacial tension, and industrial recovery separately from the collision and film-drainage mechanisms that create separable droplets (Klaffenbach et al., 2023; Kleeberg, 2022; Li et al., 2022; Milani & Timelli, 2023; Pereira, 2025a; Pereira, 2025b).

Objectives and contribution

This review therefore asks five integrated questions: (RQ1) How are liquid-metal or matte droplets generated, retained, and distinguished from chemically dissolved metal? (RQ2) How do interfacial phenomena and slag properties govern collision, film drainage, coalescence, and settling? (RQ3) How do hydrodynamic intensity, residence-time history, and dimensionless/kinetic descriptors define the window between useful coalescence and breakup? (RQ4) Which mechanisms are transferable among Al, Cu, steel, ferroalloy, Pb/Zn, Ni/Co, and complex secondary-resource systems, and how reliably do current experimental and modeling methods represent them? (RQ5) Which process interventions and scale-up criteria most plausibly reduce net metal loss? The authorial contribution is the D–I–S–H–R framework developed in Section 12.

REVIEW METHODOLOGY AND EVIDENCE APPRAISAL

Review design

The manuscript is presented as a structured critical narrative review with systematic search logic, evidence coding, and an assessment of industrial transferability. A bibliography audit confirms 108 unique entries in the retained contemporary working corpus, spanning 2020 to August 2026. The review materials identify Scopus,

Web of Science, ScienceDirect, SpringerLink, Engineering Village, and Google Scholar as intended discovery environments. Database-specific export files, complete discovery-stage hit lists, duplicate counts, exact database-by-database search dates, and record-by-record screening logs were not preserved. Accordingly, the article does not claim PRISMA-compliant systematic-review completeness and does not reconstruct missing screening counts. PRISMA 2020 is used only as a reporting benchmark for the information required to make such a claim (Page et al., 2021). Four pre-2020 foundational references are cited separately to anchor classical transport, breakup, coalescence, and population-balance concepts; they are not included in the 108-publication evidence count.

Search logic, eligibility, and extraction

The retained search vocabulary centers on combinations of "metal droplet," "metallic droplet," "slag," "molten slag," "coalescence," "settling," "entrainment," "interfacial tension," "viscosity," and "metal recovery." Eligibility was defined around direct relevance to (i) liquid metal/matte in or adjacent to slag, (ii) interfacial phenomena controlling droplet contact or separation, (iii) slag rheology or chemistry with an explicit connection to metal separation, or (iv) experimental/modeling methods that resolve these phenomena. Contextual recovery studies were retained only when they supplied industrial or process-scale constraints relevant to the reaction–coalescence–separation chain. The article therefore treats the 108 records as an audited retained corpus rather than as a statistically complete sample of all potentially discoverable literature. Because the original query strings and screening log are unavailable, no sensitivity analysis of search completeness is claimed.

Table 1 summarizes the audit fields used to distinguish mechanism, property, and scale. This is important because a high-temperature sessile-drop study and a plant settling-furnace campaign address different questions and should not be accorded the same degree of transferability.

Table 1. Review protocol and evidence-coding fields

Domain	Coding field	Purpose in synthesis
Bibliographic	Year, publication type, system	Defines scope and prevents unsupported generalization
Metal–slag system	Metal/matte, slag family, major constituents	Links observations to thermochemical context
Thermal state	Temperature, liquidus/superheat, solid fraction	Separates fully liquid from suspension behavior
Interfacial	Wetting, interfacial tension, films, reaction	Assesses contact and coalescence probability
Droplet population	Formation route, size/distribution, deformation	Connects entrainment to separability
Hydrodynamics	Mixing mode, gas rate, turbulence, residence time	Separates collision promotion from breakup
Outcome	Settling, metal recovery, residual metal, scale	Connects mechanism to process consequence
Evidence tier	A repeated industrial; B industrial/pilot; C real-system experiment; D validated model; E contextual/review	Prevents laboratory evidence from being presented as industrial proof

Note. Adapted from the review protocol supplied for this manuscript and from the reporting logic discussed by Page et al. (2021).

Table 1 emphasizes that "recovery" is not a stand-alone response variable. Without the simultaneous description of slag state, droplet population, and hydrodynamics, two reported recoveries may be physically incomparable even when the metal system is nominally the same.

Evidence hierarchy and limitations

The hierarchy used here is: A, repeated industrial operation; B, industrial or pilot campaign; C, experiment with

a real metal–slag system; D, model with explicit validation; and E, conceptual, review, thermodynamic, or contextual evidence. This hierarchy is deliberately based on transferability rather than perceived scientific quality. A carefully controlled interfacial study can provide high mechanistic confidence but still have limited direct process transfer; conversely, industrial data can demonstrate a recovery response while leaving the causal droplet-scale mechanism unresolved. Because the complete study-level extraction sheet was not retained, the manuscript does not infer or report corpus-wide A–E frequency counts. Figure 2 therefore shows the tier definitions and audit logic only; it contains no reconstructed discovery or screening numbers.

Figure 2 is placed after the methodology because the available evidence is best represented as an audited working corpus rather than as a reconstructed PRISMA funnel with invented screening counts.

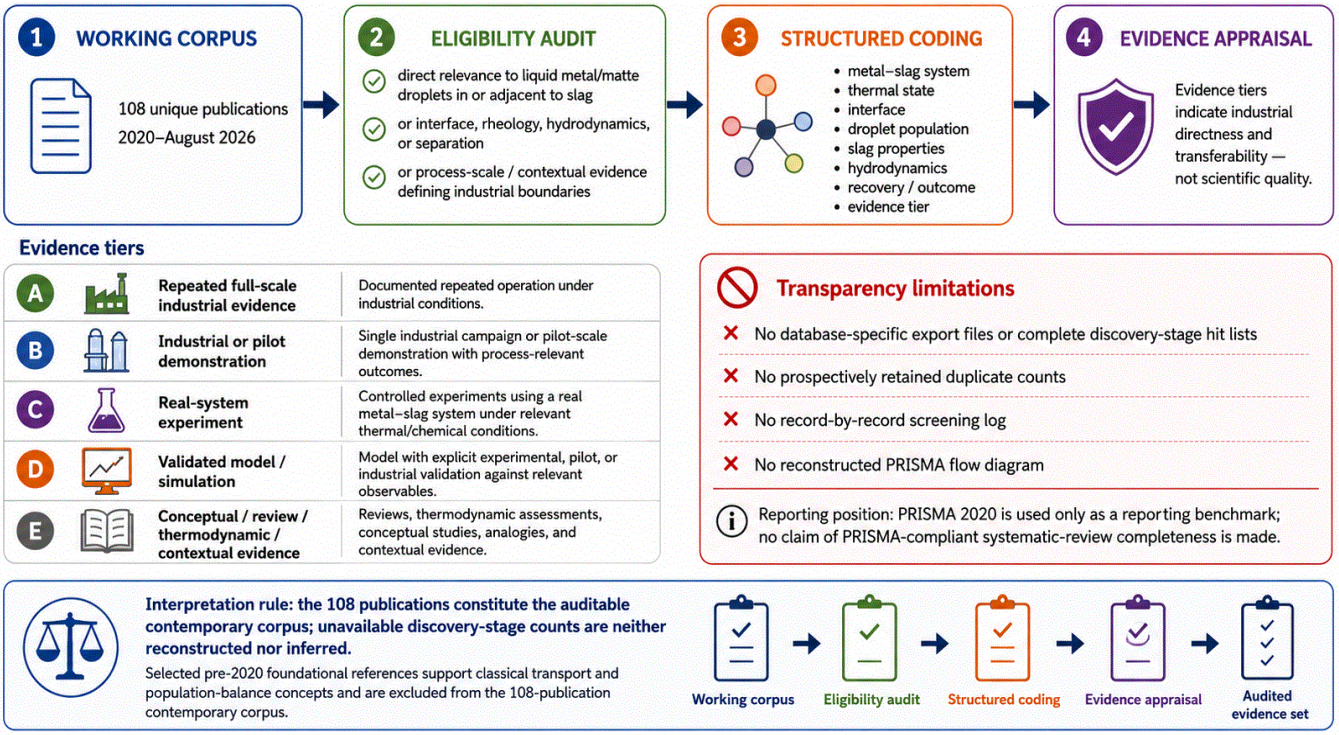

Figure 2. Working-corpus audit and evidence-appraisal logic used in the critical synthesis.

Note. Author-developed synthesis of the retained-corpus audit and evidence hierarchy. The figure deliberately avoids reconstructed discovery-stage or screening counts; PRISMA 2020 is used only as a reporting benchmark, not as a claim of systematic-review compliance (Page et al., 2021).

A further limitation is that the supplied bibliography contains complete citation metadata but not the full extraction sheet for every study. Quantitative comparisons in this review are therefore restricted to values that can be traced to the cited studies and are not extrapolated into a universal correlation. This conservative choice is preferable to creating false precision across chemically dissimilar slag systems.

ORIGIN AND NATURE OF LIQUID-METAL ENTRAINMENT IN SLAGS

Mechanical entrainment

Mechanical entrainment occurs when a pre-existing metal or matte phase is dispersed into slag by tapping, transfer, gas injection, impingement, rotational or mechanical stirring, or interfacial waves. The resulting droplets inherit a size spectrum determined by local shear, interfacial tension, and residence in the high-turbulence zone. Gas-driven systems are especially complex because bubbles both generate relative motion and deform the slag–metal interface; smaller bubbles may distribute interfacial disturbance differently from larger bubbles, while intense local turbulence promotes breakup (Chang et al., 2021; Fang et al., 2025; Kumar et al., 2020; Li & Pistorius, 2021; Liu, Cheng, et al., 2023; Liu et al., 2024; Morales et al., 2020; Natsui et al., 2020; Silva et al., 2021; Wan et al., 2024; R. Wang, Zhang, et al., 2025).

Chemical generation of metallic droplets

Droplets can also form within the slag via reduction or interfacial reactions. In such cases the problem is simultaneously chemical and hydrodynamic: nucleation or formation of metal must be followed by migration and assembly before the droplets are trapped by cooling or solids. Smelting-reduction and secondary-resource studies repeatedly show this coupling, including converter-slag iron recovery, pickling-sludge reduction, vanadium-bearing materials, coal-gasification slag, and aluminum-assisted reductions (He et al., 2020; Jing et al., 2025; Liu et al., 2026; Makhambetov et al., 2026; Mendoza et al., 2026; Nababan et al., 2024a; Nababan et al., 2024b; Wu et al., 2026; Xin et al., 2020; Xin et al., 2021; Xu et al., 2023; Xu, Liu, et al., 2022; Xu, Zhang, et al., 2022; L. Zhang & Chen, 2023).

Film fragmentation, emulsification, and droplet-size distribution

In steelmaking and converting, interfacial reactions and gas evolution can produce emulsified droplets whose lifetimes govern both the reaction and subsequent separation. Ejected droplet-size distributions and residence-time models show that generation and removal cannot be separated conceptually. Similarly, high-Al steel/flux systems and oxygen-blown copper converting demonstrate that chemical reaction can strengthen or restructure the emulsion rather than merely change equilibrium composition (Biswas et al., 2021; Biswas et al., 2022; Mitas et al., 2022; Mitas et al., 2023; Park et al., 2021; Wei et al., 2026; Xin et al., 2025; J. Zhang et al., 2023; Zhao et al., 2022).

Figure 3 is inserted here to distinguish droplet origin from droplet fate. The same final observation—metal in a solid slag sample—can arise from mechanically entrained droplets, chemically generated droplets that failed to assemble, or metal that was never a distinct liquid phase because it remained chemically dissolved.

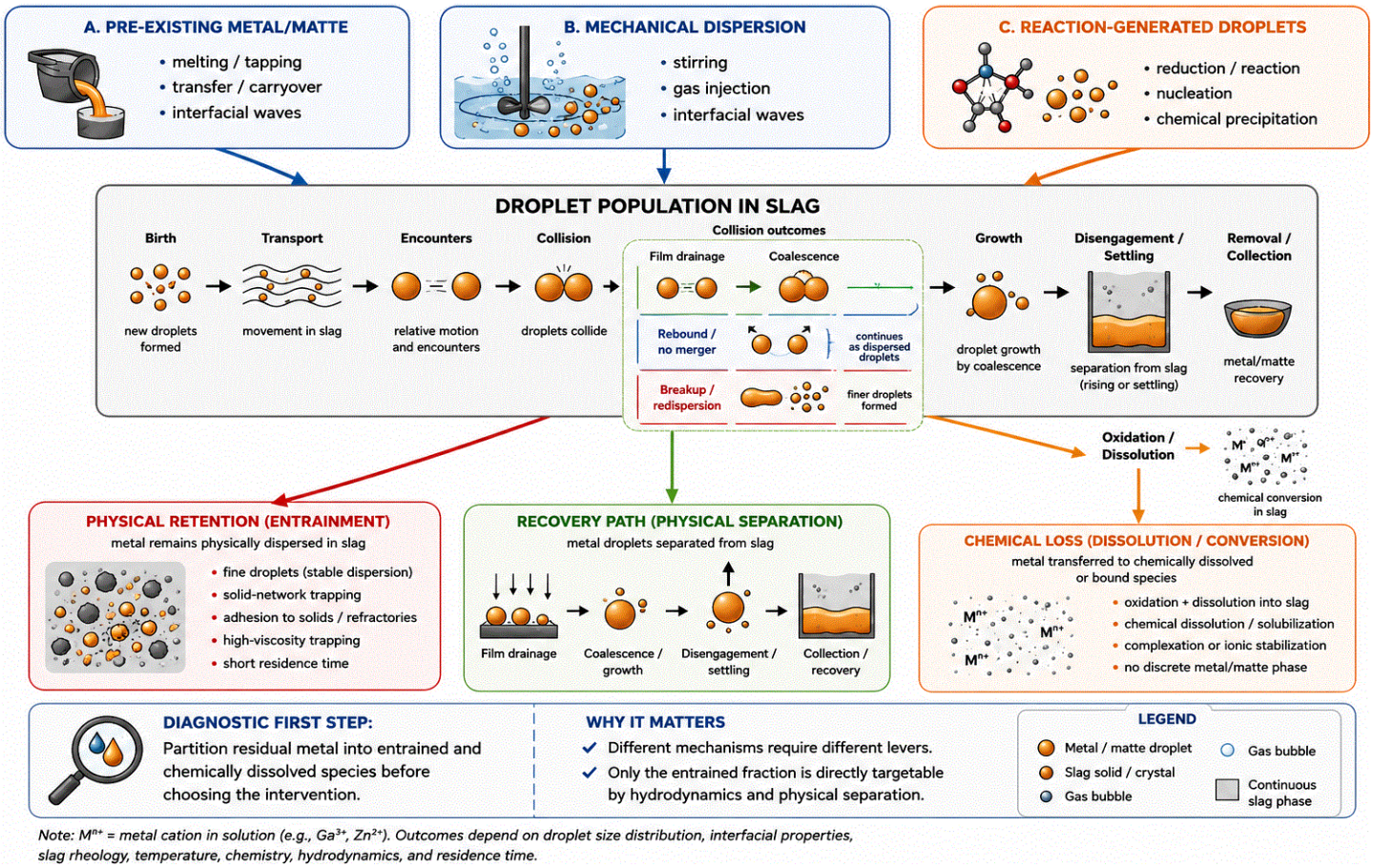

Figure 3. Generic routes for liquid-metal or matte droplet generation, growth, breakup, retention, separation, and chemical loss in metallurgical slags.

Note. Adapted from He et al. (2020), Park et al. (2021), Mitas et al. (2022, 2023), Philipson et al. (2024), and Lai et al. (2026).

The practical implication of Figure 3 is diagnostic: a slag-cleaning intervention should begin by partitioning total metal into physically entrained and chemically dissolved fractions. Coalescence-oriented interventions have little leverage over the latter unless the chemistry first creates a separate metal phase.

Distinguishing entrained from chemically dissolved metal

The distinction is particularly important in copper smelting. Industrial work explicitly separates slag-matrix copper from droplet-associated copper, while thermodynamic analyses quantify conditions under which minor elements remain dissolved in the slag phase. Similar issues arise for precious metals and complex smelting feeds, where a low residual total metal requires both favorable chemistry and efficient phase disengagement (Avarmaa et al., 2025; Isaksson et al., 2023; Isaksson et al., 2021; Klaffenbach et al., 2021; Moosavi-Khoonsari & Mostaghel, 2024; Moosavi-Khoonsari & Tripathi, 2024; Rämä et al., 2023; Romero et al., 2026; Ruismäki et al., 2020; Tian et al., 2024).

Table 2 organizes the principal entrainment pathways by diagnostic signature and the corresponding intervention.

Table 2. Mechanisms that generate or retain liquid metal in slag

Mechanism	Typical signature	Primary control	Most relevant intervention
Mechanical entrainment	Discrete droplets after tapping/stirring; broad size spectrum	Shear, waves, gas/bath interaction	Reduce entrainment source; provide calm settling stage
Chemical generation	New metal appears during reduction	Reaction rate, supersaturation, nucleation/growth	Coordinate reduction with droplet growth and separation
Emulsification/film breakup	Fine droplets concentrated near intense reaction or gas zones	Interfacial reaction, gas evolution, turbulence	Control gas rate/reaction intensity; shorten exposure to breakup zone
Interfacial-film stabilization	Droplets touch but rebound or remain separated	Oxide/solid films, surfactants, wetting	Modify chemistry/flux; increase film-drainage opportunity
Solid-network trapping	Metal enclosed by partially crystallized slag	Liquid fraction, particle morphology, yield stress	Raise superheat or alter liquidus/solid fraction
Chemical dissolution	No discrete droplet; metal located in slag matrix	Activity, oxygen potential, equilibrium	Change thermochemistry before physical separation

Note. Adapted from He et al. (2020), Park et al. (2021), Isaksson et al. (2023), Vergote et al. (2025), and Lai et al. (2026).

The table reinforces a central review principle: the correct control variable follows from the loss mechanism. Applying stronger mixing to a solid-network trapping problem, for example, can increase entrainment rather than solve it.

THERMODYNAMICS AND INTERFACIAL PHENOMENA

Surface and interfacial tension

Interfacial tension provides the capillary resistance that keeps a droplet coherent and influences deformation, breakup, wetting, and film drainage. In reactive metal–slag systems, however, it is not a fixed material constant. Oxygen, sulfur, nitrogen, fluoride-containing species, and reducible slag components can create time-dependent concentration gradients and dynamic interfacial tension. Experimental and numerical studies therefore support treating the interface as an evolving reaction zone, not as a static boundary condition (Biswas et al., 2022; Biswas et al., 2025; Bublik et al., 2021; Bublik et al., 2022; Goto et al., 2024; Li et al., 2024; Matsushita et al., 2021; Suzuki & Nakamoto, 2022; Suzuki et al., 2024; J. Wang, Fan, et al., 2025).

This dynamic behavior is consequential for modeling. A CFD calculation using one constant interfacial-tension value may reproduce bulk flow but miss transient Marangoni circulation, droplet deformation, or a shift in coalescence probability. Matsushita et al. (2021), for example, linked nitrogen-mediated interfacial gradients to Marangoni convection, while later modeling explicitly examined concentration-gradient-induced flow around steel droplets (Matsushita et al., 2021; J. Wang, Fan, et al., 2025).

Wetting, contact angle, and adhesion

Wetting determines whether metal spreads on a solid/oxide surface or tends to remain as a compact droplet. In ferroalloy systems, both alloy and slag compositions influence high-temperature wetting; sulfur and FeMn slag chemistry are therefore process variables rather than minor compositional details. In copper-smelting environments, adhesion to Fe_3O_4-rich intermediate material can physically stabilize matte or metal and impede clean disengagement (Bao et al., 2021; Bublik et al., 2021; Bublik et al., 2022; Wang et al., 2026; Xu et al., 2025).

Interfacial reactions and films

An oxide or solid film between two approaching metal droplets can suppress immediate merging even when hydrodynamic collision occurs. Aluminum is a canonical example because oxide-bearing surfaces and salt-flux chemistry strongly control whether small metallic fragments unite during remelting. In calcium-silicate reaction systems, direct observation has shown interfacial oxide-layer development together with formation and growth of Si-rich alloy droplets, demonstrating that film formation and droplet generation can be simultaneous (Çapkın & Gökelma, 2023; Milani & Timelli, 2023; Milani et al., 2023; Philipson et al., 2024; Vallejo-Olivares et al., 2022; Wan et al., 2020).

Figure 4 is inserted at this point because the decisive step is the thin film between contacting droplets. The relevant comparison is between contact duration and the time required for the intervening film to drain and rupture.

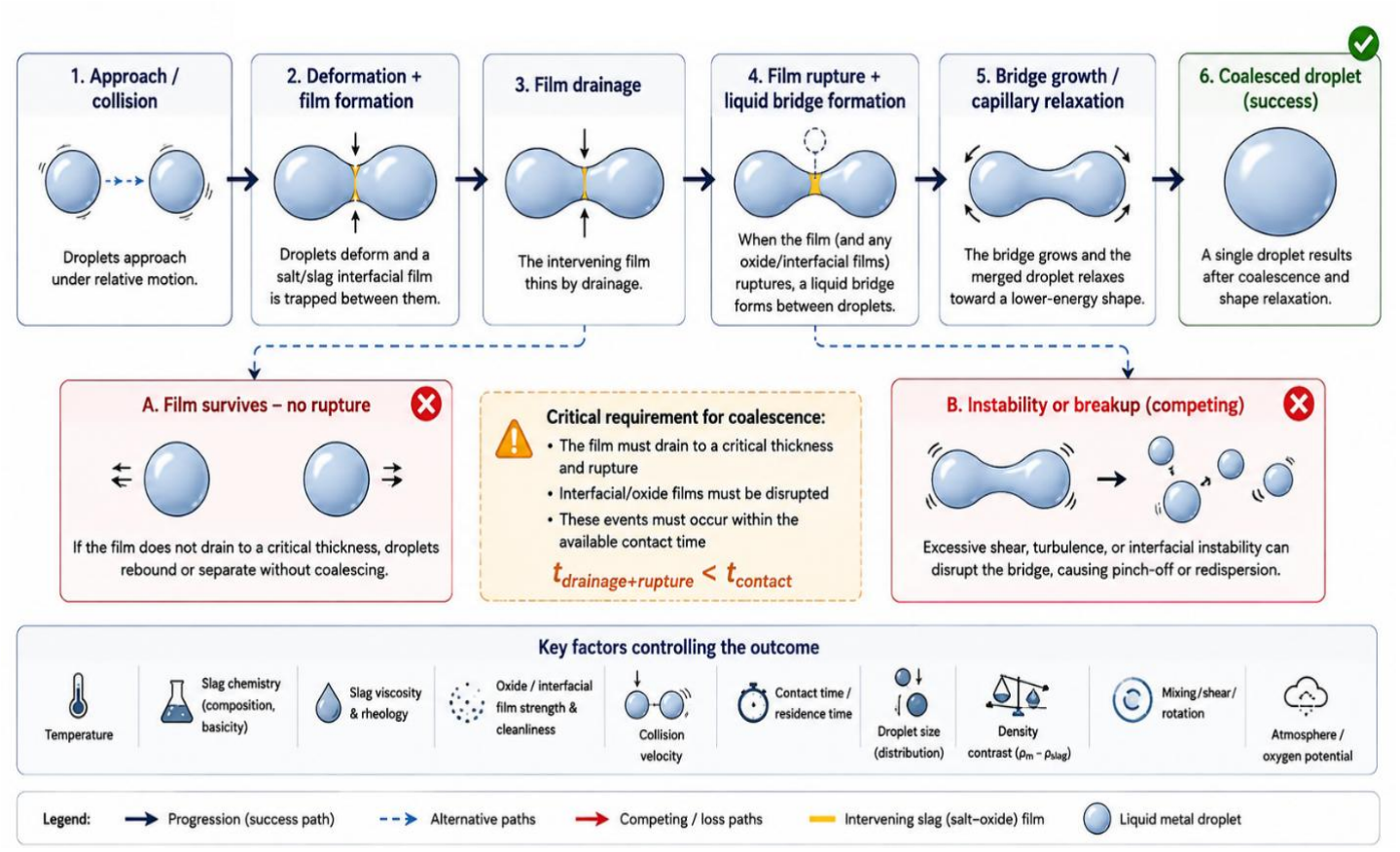

Figure 4. *Conceptual collision–deformation–film drainage–film rupture–coalescence sequence.*

Note. Adapted from thin-film and droplet-coalescence concepts discussed by Mirjalili and Chan (2021), McGuan et al. (2022), Pelusi et al. (2023), Qian et al. (2023), and Lai et al. (2026).

The sequence in Figure 4 explains why increasing collision frequency alone is insufficient. If interface-active species or oxide films increase the drainage/rupture time beyond the contact time, the process results in repeated encounters, rebounds, or partial coalescence rather than durable droplet growth.

Spreading and separation coefficients: useful but incomplete descriptors

Spreading or separation coefficients can summarize static interfacial energy balances, but critical interpretation is required because metallurgical interfaces are reactive and often chemically nonuniform. A favorable static wetting criterion does not account for transient adsorption, interfacial reaction products, Marangoni stresses, or solids at the interface. The highest-confidence use of these coefficients is therefore comparative within a defined chemical system, not as universal predictors across slag families (Bao et al., 2021; Goto et al., 2024; Matsushita et al., 2021; Pelusi et al., 2023; Philipson et al., 2024; Suzuki & Nakamoto, 2022; Suzuki et al., 2024; Xu et al., 2025).

SLAG PROPERTIES CONTROLLING COALESCENCE

Viscosity and rheology

Viscosity controls at least three linked phenomena: the translational mobility of droplets, the rate at which the inter-droplet film drains, and the hydrodynamic damping of deformation and turbulence. It therefore appears repeatedly as a first-order variable in copper-slag cleaning, iron-droplet settling, and secondary-resource recovery. Yet viscosity cannot be interpreted independently of temperature, composition, and solids because these determine whether the slag is a Newtonian liquid or a suspension with non-Newtonian behavior (Eguchi et al., 2023; Isaksson et al., 2023; Madej, 2025; Vergote et al., 2025; Q.-M. Wang, Huang, et al., 2023; Wu et al., 2026).

The strongest quantitative industrial anchor in the working corpus is the CaO-modified copper-smelting study by Isaksson et al. (2023). Across industrial batches, higher CaO lowered slag viscosity, shifted the copper droplet-size distribution toward larger droplets, and increased overall copper recovery from 63% to 88% as viscosity decreased from 0.51 to 0.25 Pa·s. This is not evidence that "lower viscosity is always better"; rather, it demonstrates the coupled pathway viscosity → mobility/growth → separation under a particular iron-silicate chemistry and operating window (Isaksson et al., 2023).

Density contrast, liquidus, superheat, and solid fraction

The density difference between metal and slag supplies the gravitational driving force, but the usable force depends on whether the slag remains sufficiently fluid. Subliquidus operation introduces crystals or solid networks that can raise apparent viscosity and physically trap droplets. Recent rheological work on slag–melilite suspensions highlights the additional role of solid-particle shape and volume fraction, showing why a simple temperature–viscosity curve for a fully liquid slag may fail in an industrial bath (Vergote et al., 2025).

Spinel-bearing nonferrous slags and other partially crystallized systems require particular caution because the onset and morphology of solids can transform the separation regime. Likewise, the liquid-phase fraction in semi-molten reduction controls whether newly formed metal can assemble and migrate (Jing et al., 2025; Kleeberg, 2022; Park et al., 2026; Tian et al., 2026).

Slag structure, basicity, and major oxides

In silicate slags, network formers and modifiers control structural polymerization and thereby viscosity. CaO, MgO, Al_2O_3, SiO_2, and FeO_x cannot therefore be treated only as bulk composition entries; their influence depends on oxidation state, liquidus relationships, and the location of the composition relative to phase boundaries. Experimental viscosity studies and copper-slag modification work show that additive effects can be strongly temperature dependent, especially when structural change or solid precipitation begins (Eguchi et al., 2023; Isaksson et al., 2023; Liu, Xu et al., 2023; Madej, 2025; Tian et al., 2026; Wu et al., 2026).

Table 3 summarizes the directional effects that are mechanistically robust while flagging the conditions under which the expected trend can reverse.

Table 3. Slag properties that control droplet mobility, collision, and separation

Property	Primary mechanism	Expected favorable direction	Critical caveat
Viscosity / apparent viscosity	Drag + film drainage + damping	Lower, within stable liquid region	May signal changed chemistry or approach to liquidus; non-Newtonian suspensions invalidate simple correlations
Metal–slag density contrast	Gravitational driving force	Higher contrast	Drag and droplet deformation can dominate for small droplets
Solid fraction/yield behavior	Mechanical trapping + high apparent viscosity	Lower solid fraction	Some solids also alter interfacial films and nucleation
Liquidus / superheat	Controls fluid fraction and crystallization	Adequate superheat	Higher temperature can increase reaction, oxidation, refractory wear, and energy use
Basicity/network modification	Changes silicate structure and viscosity	System-specific optimization	Can change metal solubility and phase equilibria
FeO_x / redox state	Viscosity + reaction + metal solubility	System-specific	Reduction may create droplets while changing viscosity simultaneously
Interfacial-active constituents	Dynamic interfacial tension / Marangoni flow	Not monotonic	Initial and equilibrium effects can differ

Note. Adapted from Eguchi et al. (2023), Isaksson et al. (2023), Kleeberg (2022), Vergote et al. (2025), Suzuki and Nakamoto (2022), and Suzuki et al. (2024).

The most transferable conclusion from Table 3 is not a universal target value but a hierarchy: first ensure a predominantly liquid and mobile slag; then optimize viscosity and interface chemistry within the phase-stable operating window.

DROPLET DYNAMICS AND COALESCENCE MECHANISMS

Droplet motion and collision

A droplet moving through slag experiences gravity, buoyancy, drag, pressure and inertial forces, interfacial stresses, and—when present—turbulent fluctuations or bubble-induced motion. Collision can arise from differential settling, turbulent relative velocity, shear, wake capture, or converging flows. Experimental liquid–liquid studies show that the outcome changes with impact velocity: increasing velocity can move the system from coalescence to coalescence with rebound and then to rebound, demonstrating that collision efficiency and coalescence efficiency are separate quantities (Qian et al., 2023).

Film drainage, rupture, and partial coalescence

After contact, the thin intervening slag or film must drain. Drainage is resisted by viscosity and can be stabilized by surface-active species, oxide skins, or particles. The eventual outcome may be complete coalescence, partial coalescence, bouncing, or separation without merging. Room-temperature liquid-metal analog experiments provide especially clear evidence that partial coalescence can create daughter droplets and a cascade whose termination depends on the balance between capillary and viscous effects (McGuan et al., 2022; Mirjalili & Chan, 2021; Pelusi et al., 2023).

Breakup versus coalescence

The steady droplet-size distribution is set by a population balance between birth, growth, breakup, and removal. Intensifying flow usually increases collision frequency, but the same increase in shear and turbulent energy can deform and fragment droplets. Numerical work on metal–slag emulsions, industrial side-blown smelting, and

gas-stirred reactors makes this competition explicit: regions of strong turbulence are also regions in which bubble and droplet deformation or breakup becomes more likely (Fang et al., 2025; Li et al., 2024; Li & Pistorius, 2021; Wan et al., 2024; Zhang et al., 2026).

Figure 5 is placed here to formalize this competition. It is a conceptual map rather than a fitted universal curve; its purpose is to identify the finite operating region in which collision/coalescence can outpace breakup.

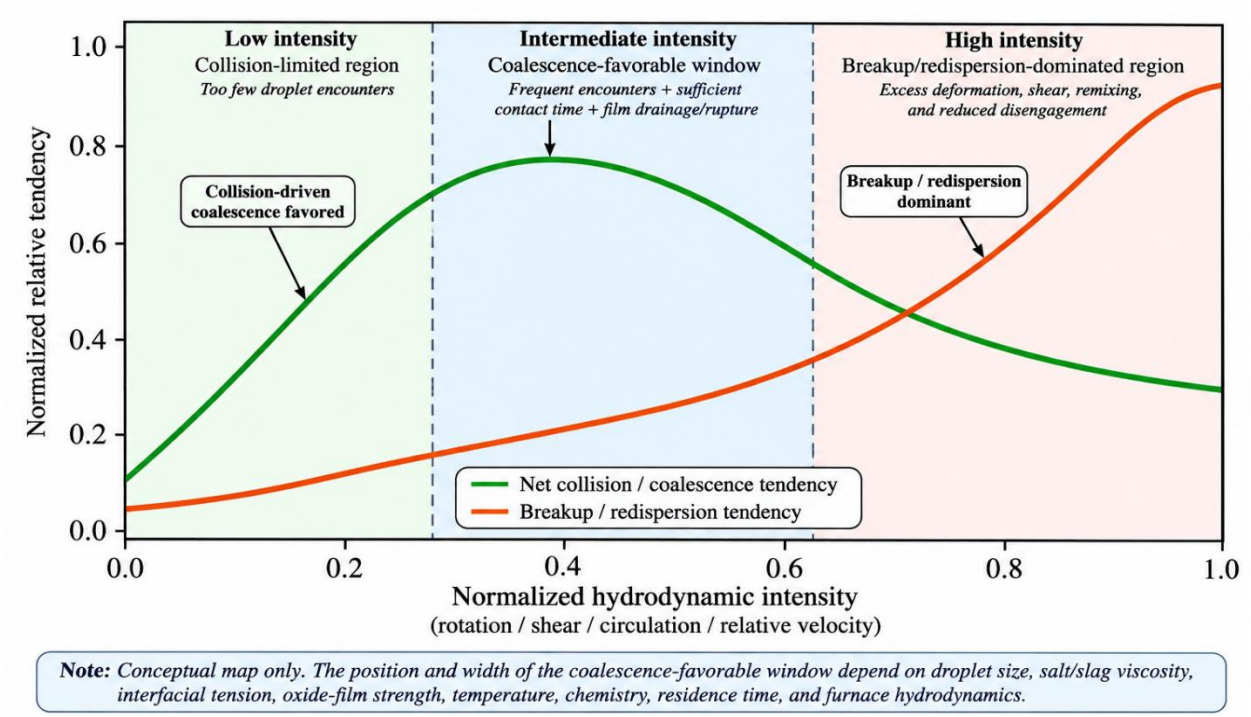

Figure 5. *Conceptual competition between collision/coalescence and breakup in determining characteristic droplet size.*

Note. Adapted from coalescence/bouncing observations and multiphase-flow analyses by McGuan et al. (2022), Qian et al. (2023), Li et al. (2024), Fang et al. (2025), and Zhang et al. (2026).

The review therefore rejects a one-directional "agitation improves coalescence" rule. Agitation is beneficial only if it raises the effective collision kernel more than it raises the breakup kernel, and if enough subsequent low-turbulence time remains for enlarged droplets to separate.

Population-balance perspective

Population-balance modeling is a natural framework because it treats the droplet distribution, rather than a single average diameter, as the state variable. In metallurgical applications, the balance should contain source terms for reaction-generated droplets and mechanical entrainment, coalescence kernels, breakup frequencies and daughter-size distributions, and removal by settling or tapping. In schematic form, the evolution can be written as a competition among generation, coalescence, breakup, and removal (Coulaloglou & Tavlarides, 1977; Prince & Blanch, 1990). Existing studies of ejected size distributions, residence times, and droplet assembly provide elements of this description, but an experimentally validated, chemistry-aware population balance for industrial slag cleaning remains uncommon (Lai et al., 2026; Mitas et al., 2022; Mitas et al., 2023; Wei et al., 2026; Xin et al., 2025).

$$\partial n(d,t)/\partial t = Bgen + Bcoal + Bbreak - Dcoal - Dbreak - Rsep$$

where n(d,t) is the droplet-size population density; B and D denote birth and death terms; and Rsep represents removal by gravitational or forced separation. A useful decomposition of the coalescence kernel is $K_{ij} = \beta_{ij} E_{ij}$, where β_{ij} is the collision frequency and E_{ij} is the probability that a collision produces durable coalescence. Turbulence, shear, differential settling, and bubble-induced motion primarily affect β_{ij}, whereas film drainage,

oxide/solid films, dynamic interfacial tension, and contact duration strongly affect Eij. Classical breakup theory similarly links increasing turbulent stress and Weber number to a rising breakup tendency (Hinze, 1955).

Characteristic-time criteria for successful coalescence and separation

Two time-scale ratios make the kinetic competition explicit. For droplet contact, $\Pi c = t_{drain}/t_{contact}$ compares the time required for the intervening film to drain and rupture with the duration of contact: $\Pi c < 1$ is coalescence-favorable, whereas $\Pi c > 1$ favors rebound, partial coalescence, or separation. After droplet growth, $\Pi s = t_{sep}/t_{hold}$ compares the time required for gravitational or forced disengagement to the available holding time; net recovery requires that Πs remain below unity before tapping or solidification. These ratios are conceptual rather than universal constants because viscosity, solids, interfacial reaction, droplet size, and local turbulence all shift the underlying characteristic times.

HYDRODYNAMICS, MIXING, AND RESIDENCE TIME

Quiescent settling and deliberate holding

Quiescent or low-turbulence holding converts droplet growth into separation. Once a droplet becomes large enough, continued intense mixing is no longer required and can be counterproductive. Settling-furnace practice, generic sedimentation studies, and residence-time modeling all support treating “mix” and “settle” as separate stages or at least separate hydrodynamic zones (Isaksson et al., 2023; Isaksson et al., 2021; Mitas et al., 2023; Qian et al., 2023; Q.-M. Wang, Huang, et al., 2023).

Mechanical stirring

Mechanical stirring can improve recovery by accelerating the reaction and increasing the encounter rate among small droplets, as demonstrated in converter-slag smelting-reduction work. The benefit is conditional: excessive intensity or duration can produce a finer emulsion, and stopping agitation too late can leave insufficient settling time for the newly enlarged droplets to settle (He et al., 2020; Lai et al., 2026).

Gas stirring and bubble-mediated transport

Gas stirring introduces another phase and, therefore, another set of collision and deformation mechanisms. Bubble size, plume structure, slag-eye formation, and bubble penetration through the interface determine whether gas promotes transport, inclusion capture, interfacial renewal, or undesirable emulsification. Smaller bubbles can distribute surface impact and suppress large slag-eye formation at a given gas rate, whereas high-turbulence zones in side-blown systems promote breakup and strong interfacial mixing (Chang et al., 2021; Cheng et al., 2024; Fang et al., 2025; Kumar et al., 2020; Li & Pistorius, 2021; Liu, Cheng, et al., 2023; Liu et al., 2024; Morales et al., 2020; Wan et al., 2024; R. Wang, Zhang, et al., 2025).

Rotary, electromagnetic, and forced-flow approaches

Rotary processing is especially important in aluminum recycling because it combines heat transfer, salt-flux contact, oxide-film disruption, and metal collection. Electromagnetic or other forced-flow strategies are less represented in the supplied corpus as direct coalescence studies, but the same design question applies: does the imposed flow create useful collisions and transport without locking the system into a high-breakup dispersion? Industrial recycling experience and salt-flux studies provide the most direct evidence base for aluminum (Milani & Timelli, 2023; Milani et al., 2023; Pereira, 2025a; Pereira, 2025b; Pichat et al., 2020; Vallejo-Olivares et al., 2022; Wan et al., 2020).

The mixing–residence-time paradox

Figure 6 is inserted here because the process variable is not mixing alone but the sequence of mixing intensity and residence time. A practical operating cycle often requires an active period that promotes reaction and encounters followed by a quieter period that allows separation.

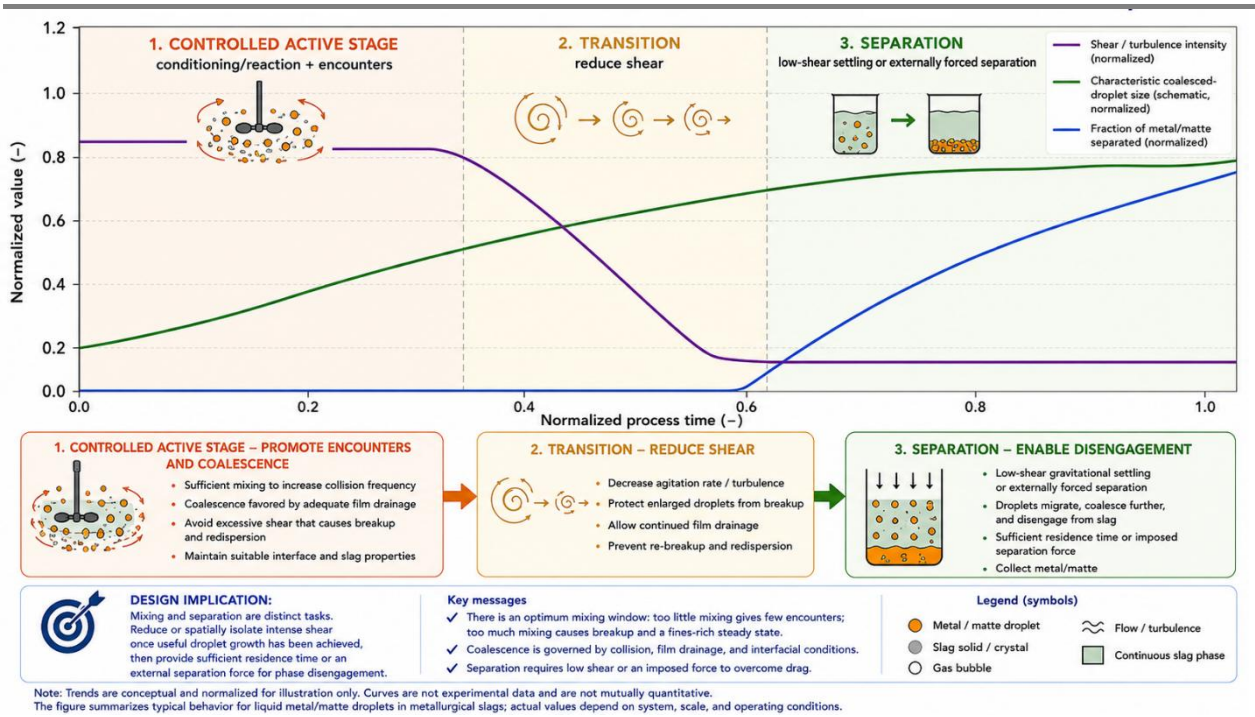

Figure 6. Staged hydrodynamic sequence separating an active collision/coalescence period from a subsequent low-turbulence or forced-separation period.

Note. Author-developed conceptual synthesis based on mechanical-stirring, gas–slag interfacial, and multiphase-flow evidence reported by He et al. (2020), Chang et al. (2021), Morales et al. (2020), Fang et al. (2025), and Zhang et al. (2026). The trajectories are qualitative and are not fitted universal kinetics.

The staged sequence shown in Figure 6 is system-specific. The useful duration and intensity of the active period vary with viscosity, droplet size, density contrast, solids content, gas rate, geometry, and reaction kinetics. The key design point is temporal or spatial separation of tasks: collision promotion is favored during the active stage, whereas droplet preservation and phase disengagement are favored after the intensity is reduced. This is why a universal rpm, gas flow, or power density criterion is unlikely to be transferable without dimensionless, population-level, and residence-time normalization.

QUANTITATIVE DESCRIPTION AND DIMENSIONLESS ANALYSIS

Settling velocity and its limits

For a spherical droplet in creeping flow, Stokes' law provides the familiar first estimate of terminal velocity:

$$u_t = (\Delta\rho\, g\, d^2) / (18\, \mu_s)$$

where u_t is terminal velocity, $\Delta\rho$ is the metal–slag density difference, g is gravitational acceleration, d is droplet diameter, and μ_s is slag viscosity. The relation makes the importance of droplet growth transparent because velocity scales with d^2, and it also shows why lowering viscosity can be powerful. However, direct use is restricted to low-Reynolds-number , approximately spherical particles/droplets, dilute dispersions, and Newtonian continuous phases. Real slags may violate every one of these assumptions (Qian et al., 2023; Vergote et al., 2025; Q.-M. Wang, Huang, et al., 2023).

For a clean mobile liquid droplet in creeping flow, internal circulation gives the Hadamard–Rybczynski correction (Clift et al., 1978):

$$uHR = (\Delta\rho\, g\, d^2 / 6\, \mu_s)\, [(\mu_s + \mu m)/(2\, \mu_s + 3\, \mu m)]$$

where μm is the viscosity of the dispersed metal/matte phase. The expression approaches the rigid-sphere Stokes result as $\mu m/\mu_s$ becomes very large and predicts greater mobility when the interface remains clean and mobile. In

metallurgical slags, reactive films, surfactants, particles, and Marangoni stresses can partially immobilize the interface, so Stokes and Hadamard–Rybczynski are best treated as mechanistic bounds rather than direct plant correlations. At finite Reynolds number, with deformation, concentrated dispersions, walls, or non-Newtonian/yield-stress slags, drag must be evaluated with regime-appropriate correlations or direct simulation.

Dimensionless groups

A more transferable description uses dimensionless groups that compare the relevant force scales. Reynolds number characterizes inertia relative to viscosity; Weber number compares inertia with interfacial tension; Eötvös/Bond number compares buoyancy or gravity with capillarity; Capillary number compares viscous stress with capillarity; Ohnesorge number combines viscosity, density, size, and interfacial tension and is particularly useful for coalescence/partial-coalescence regimes; and Morton number characterizes a fluid pair independently of droplet size. The classical Hinze breakup concept emphasizes a critical Weber-type competition between turbulent stress and capillarity, while modern metallurgical applications must additionally account for reactive interfaces and evolving rheology (Hinze, 1955; McGuan et al., 2022; Qian et al., 2023; Q.-M. Wang, Huang, et al., 2023). These groups do not replace chemistry, but they help separate geometric scale from physical regime.

Table 4 summarizes these groups and the metallurgical question each one answers.

Table 4. Dimensionless groups for droplet behavior in molten slag

Group	Definition	Physical comparison	Use / warning
Reynolds, Re	$\rho_s u d / \mu_s$	Inertia / viscous force	Identifies creeping, transitional, or inertial motion; local turbulence complicates interpretation
Weber, We	$\rho_s u^2 d / \gamma_{m-s}$	Inertia / capillarity	Higher We increases deformation and breakup propensity
Eötvös (Bond), Eo	$\Delta\rho g d^2 / \gamma_{m-s}$	Gravity / capillarity	Indicates shape deformation by buoyancy/gravity
Capillary, Ca	$\mu_s u / \gamma_{m-s}$	Viscous stress / capillarity	Relevant to deformation and film drainage
Ohnesorge, Oh	$\mu_s / \sqrt{(\rho_s \gamma_{m-s} d)}$	Viscous / inertial-capillary effects	Useful for coalescence and partial-coalescence regime changes
Morton, Mo	$g \mu_s^4 \Delta\rho / (\rho_s^2 \gamma_{m-s}^3)$	Fluid-pair property combination	Useful for comparing systems but sensitive to high-temperature property uncertainty

Note. Adapted from the droplet-dynamics framework used in McGuan et al. (2022), Qian et al. (2023), and Wang et al. (2023). Symbols: ρ_s, slag density; μ_s, slag viscosity; γ_{m-s}, metal–slag interfacial tension.

The primary limitation is uncertainty in high-temperature properties, especially dynamic interfacial tension and suspension rheology. Dimensionless analysis is most useful when the properties are measured or consistently estimated for the actual slag composition rather than imported from generic values.

From single-droplet equations to industrial distributions

Industrial recovery depends on a distribution of d, not a single d. Because settling rate is nonlinear in size, a small mass fraction of fine droplets can dominate residual metal after the coarse fraction has already separated. This provides a mechanistic explanation for why droplet-size-distribution measurements should accompany total residual-metal assays in slag-cleaning trials. Stokes and Hadamard–Rybczynski relations provide useful limiting concepts for single droplets, but population-level recovery additionally depends on coalescence/breakup kernels, hindered transport, non-Newtonian rheology, and residence-time distribution. Industrial copper-slag work that combines viscosity, droplet-size distribution, slag-matrix copper, and total recovery is therefore a stronger template than reporting a single final Cu concentration (Isaksson et al., 2023).

EFFECTS OF TEMPERATURE, CHEMISTRY, AND PROCESS ADDITIVES

Temperature and oxygen potential

Temperature simultaneously changes viscosity, liquid fraction, diffusion, reaction rate, interfacial tension, and the thermodynamic stability of dissolved versus metallic species. Increasing temperature may therefore improve droplet mobility while increasing oxidation, dissolution, volatile losses, or refractory interaction. Oxygen potential is equally coupled: it can control whether a metal exists as a separate droplet and also alter the adsorption state and interfacial tension of the metal–slag boundary (Biswas et al., 2021; Biswas et al., 2022; Goto et al., 2024; Klaffenbach et al., 2021; Matsushita et al., 2021; Moosavi-Khoonsari & Mostaghel, 2024; Moosavi-Khoonsari & Tripathi, 2024; Park et al., 2026; Spooner et al., 2020).

Flux and slag modifiers

Additives are attractive because they can shift several properties at once. In industrial copper slag, CaO modification reduced viscosity and increased droplet size and recovery. In FeO_x–SiO_2 melts, CaO, MgO, and Al_2O_3 change viscosity through structural and phase-equilibrium effects. In aluminum salt fluxes, cryolite changes both melting behavior and coalescence: up to approximately 3 wt% cryolite, increased addition improved coalescence of remelted coated chips, while differences above that level were minor in the cited study (Eguchi et al., 2023; Isaksson et al., 2023; Milani et al., 2023).

The key critical point is diminishing return and multi-objective trade-off. A modifier should be evaluated not only for viscosity reduction but also for liquidus margin, interfacial chemistry, metal solubility, refractory compatibility, emissions, salt consumption, and downstream slag valorization (Klaffenbach et al., 2023; Liu, Xu, et al., 2023; Milani & Timelli, 2023; Wan et al., 2020).

Interfacial-active elements

Dynamic interfacial-tension studies demonstrate why "same viscosity" does not mean "same coalescence." Sulfur modifies ferroalloy interfaces, nitrogen can drive Marangoni circulation in iron–slag systems, B_2O_3 changes the transient interfacial-tension trajectory by participating in oxygen transfer, and fluoride ions can lower the initial iron–slag interfacial tension even when slags are designed for similar SiO_2 activity and viscosity. At higher fluoride content, later-time behavior can reverse because volatilization and changing activity alter the interface (Bublik et al., 2021; Matsushita et al., 2021; Suzuki & Nakamoto, 2022; Suzuki et al., 2024).

Table 5 presents the numerical anchors that can be traced directly in the retained manuscript, along with mechanistic modifier evidence. Values are intentionally not pooled because the systems, temperatures, compositions, and scales are not harmonized.

Table 5. Representative quantitative and mechanistic anchors for chemistry, additives, and force intensification

System/intervention	Traceable response / numerical anchor	Process interpretation	Transferability caveat
Industrial Cu iron-silicate slag + CaO	Viscosity decreased; droplet distribution shifted larger; recovery 63→88% as viscosity 0.51→0.25 Pa·s	Strong industrial evidence that fluidity and droplet growth can translate to recovery	Temperature/solid-precipitation sensitivity at higher CaO; chemistry-specific
NaCl–KCl flux + cryolite for Al chips	Liquidus decreased experimentally; coalescence improved up to ~3 wt% cryolite; little extra benefit above	Shows flux chemistry can disrupt barriers and improve collection	Fluoride/salt management and diminishing returns
FeO_x–SiO_2 + Al_2O_3/CaO/MgO	Viscosity changes depend on modifier and temperature	Can shift droplet mobility and settling	Must be interpreted with phase equilibria and liquid fraction

System/intervention	Traceable response / numerical anchor	Process interpretation	Transferability caveat
Liquid Fe / silicate slag + B_2O_3	Dynamic interfacial-tension trajectory changed	Can alter film drainage and Marangoni response	Reactive, time-dependent interface; not a simple constant γ
Liquid Fe / silicate slag + fluoride	Initial interfacial tension lower; later behavior affected by fluoride volatilization/activity changes	Potentially changes wetting/coalescence dynamics	Volatilization and composition drift complicate steady-state interpretation
Molten Cu slag/matte under supergravity	Cu recovery reported at 96.79%; residual Cu in slag <0.11 wt% in the cited study	Large external body force can bypass slow gravitational settling	Scale-up, equipment, energy, and integration constraints

Note. Adapted from Isaksson et al. (2023), Eguchi et al. (2023), Milani et al. (2023), Suzuki and Nakamoto (2022), Suzuki et al. (2024), and Z. Wang, Gao, et al. (2025). Numerical values are reported only where explicitly traceable in the cited evidence; blank or qualitative entries should not be interpreted as zero effect.

Table 5 shows two distinct levers: property conditioning and force intensification. The former changes the droplet/slag system itself; the latter changes the separation driving force. The strongest process designs may combine both but should avoid using force intensification to compensate for a fundamentally immobile or partially solid slag.

METAL-SPECIFIC EVIDENCE

Aluminum and aluminum-rich slags/dross

Aluminum recovery is dominated by an unusually strong interfacial-film problem because oxide skins can isolate metallic fragments even when they are in close contact. Salt fluxes therefore serve not only as thermal media but also as interfacial and oxide-management agents. Remelting studies, salt-flux reviews, cryolite-addition work, decoating research, and flux-composition analysis consistently place surface cleanliness and salt chemistry alongside temperature and mixing as primary determinants of coalescence (Çapkın & Gökelma, 2023; Milani & Timelli, 2023; Milani et al., 2023; Pichat et al., 2020; Vallejo-Olivares et al., 2022; Wan et al., 2020).

The recent direction toward supergravity and integrated hot-dross processing shifts the emphasis from relying solely on spontaneous coalescence to combining droplet/particle conditioning with a stronger separation force. Studies on aluminum dross, chips, and Al–Zn bottom slag show this broader move toward intensified physical separation and salt reuse (Lan et al., 2026; Sun et al., 2024; Sun et al., 2025; Z. Wang, Gao, et al., 2023; Wang et al., 2024; Xu et al., 2025).

Aluminum also appears as a reductant or reaction participant in non-aluminum slags, where the newly generated metallic phase and interfacial oxide products complicate the simple “aluminum recycling” picture. Aluminothermic battery and vanadium/steel-slag studies, as well as direct Al–calcium-silicate interface observations, are relevant to the general mechanism of reaction-generated droplet assembly (Nababan et al., 2024a; Nababan et al., 2024b; Philipson et al., 2024; Xin et al., 2021; Xu et al., 2023; Xu, Liu, et al., 2022; Xu, Zhang, et al., 2022; L. Zhang & Chen, 2023).

Copper slags and matte-bearing systems

Copper slags provide the clearest industrial bridge between droplet-scale physics and plant recovery. Industrial settling studies identify viscosity, droplet-size distribution, and the split between dissolved and entrained Cu as joint variables. CaO and Na_2O modifications, Fe_3O_4-rich interfacial structures, gas–slag–matte hydrodynamics, and supergravity separation all target different bottlenecks in the same chain (Chi et al., 2024; Isaksson et al., 2023; Isaksson et al., 2021; Klaffenbach et al., 2023; Klaffenbach et al., 2021; Liu, Xu, et al., 2023; Madej, 2025; Tian et al., 2024; Wan et al., 2024; Wang et al., 2026; Z. Wang, Gao, et al., 2025; Xu et al., 2025; Zhou et al., 2026).

The most important warning is that "copper in slag" can represent metal, matte/sulfide droplets, or dissolved copper, so an intervention that improves settling of one phase may not change the chemically dissolved fraction. Complex feeds such as WEEE, spent catalysts, and mixed slags add collector-metal and impurity effects that must be included in the phase-separation analysis (Gu et al., 2025; Heo et al., 2022; Moosavi-Khoonsari & Tripathi, 2024; Romero et al., 2026; Tsebe & Steenkamp, 2024; Zhu et al., 2025).

Steelmaking and iron-bearing slags

Steelmaking offers extensive evidence on emulsification, decarburizing droplets, slag–metal dispersion, and hydrodynamic modeling. In this domain, droplets are often valuable reaction sites during refining, so the process objective can be temporally opposite: first create or maintain an emulsion for mass transfer, then destroy it for clean separation. Decarburization studies, RH/ladle work, ejected-droplet models, and BOF residence-time analyses therefore provide important transferable concepts even when the immediate goal is not slag cleaning (Biswas et al., 2021; Biswas et al., 2022; Li et al., 2022; Liu, Cheng, et al., 2023; Liu et al., 2024; Mitas et al., 2022; Mitas et al., 2023; Morales et al., 2020; Schubert et al., 2022; Silva et al., 2021; Wei et al., 2026; Xin et al., 2025; J. Zhang et al., 2023; Zhao et al., 2022).

Iron recovery from converter slag, pickling sludge, oolitic ores, gasifier slags, and vanadium-bearing materials further demonstrates how reduction-generated droplets must grow in a chemically evolving slag. These studies support the population-balance view in which droplet generation and removal occur simultaneously (He et al., 2020; Hu et al., 2025; Jing et al., 2025; Lai et al., 2026; Lin et al., 2021; Liu et al., 2026; Mendoza et al., 2026; Wu et al., 2026; Xin et al., 2020; Xu et al., 2023).

Ferroalloys, lead/zinc, nickel, cobalt, PGM, and complex systems

Ferroalloy slags emphasize wetting and interface chemistry: sulfur and FeMn slag composition measurably change interfacial behavior, while tapping models and hydrogen pre-reduction studies show the importance of flow and reaction history (Bao et al., 2021; Bublik et al., 2021; Bublik et al., 2022; Kumar & Safarian, 2025; Makhambetov et al., 2026; Tangstad et al., 2022).

Lead/zinc and nickel/cobalt/PGM systems expand the relevance of rheology, reductant selection, and collector-phase formation. Secondary lead slags can operate as solid-bearing suspensions with strong rheological effects; zinc-leach and smelting slags require reduction to create or enlarge a separable metal phase; nickel slag cleaning and catalyst/e-waste co-treatment show how metal recovery depends on both thermodynamics and a collector/separation mechanism (Martín Treceño et al., 2021; Rämä et al., 2023; Ruismäki et al., 2020; Tian et al., 2026; Vergote et al., 2025; Gu et al., 2025; Mongoljiibuu et al., 2025; Romero et al., 2026; Tsebe & Steenkamp, 2024). Boundary evidence from thermodynamic smelting assessments, recovery of precious and base metals from complex residues, and combined waste/slags confirms that droplet coalescence must ultimately be embedded in a complete reaction-and-separation flowsheet rather than optimized in isolation (Schrama et al., 2021).

Table 6 compares the dominant bottleneck by system rather than implying that one optimum viscosity, interfacial tension, or mixing condition applies universally.

Table 6. Cross-system comparison of droplet-coalescence and separation constraints

System	Characteristic interface/slag issue	Dominant droplet-scale bottleneck	Most transferable recovery lesson	Selected evidence
Al/salt flux/dross	Oxide films; salt chemistry; low metal density	Film disruption + collection of small metallic fragments	Condition interface, then apply calm or forced separation	Çapkın & Gökelma; Milani & Timelli; Milani et al.; Z. Wang, Gao, et al.; Lan et al.
Cu / iron-silicate slag	Dissolved vs entrained Cu; Fe_3O_4/spinel; matte droplets	Viscosity + droplet size + adhesion	Measure matrix Cu and droplet size; condition slag before settling	Isaksson et al.; Chi et al.; Xu et al.; G. Wang et al.; Z. Wang, Gao, et al.

System	Characteristic interface/slag issue	Dominant droplet-scale bottleneck	Most transferable recovery lesson	Selected evidence
Steel / BOF / ladle	Reactive emulsion; gas plumes; surfactants	Desired emulsion during reaction, unwanted persistence afterward	Separate reaction-stage mixing from post-reaction disengagement	Biswas et al.; Mitas et al.; Liu et al.; Zhang et al.
Fe / smelting reduction	Droplets generated inside slag during reduction	Assembly rate versus slag solidification/viscosity	Coordinate reaction, coalescence, and settling time	He et al.; Lai et al.; Hu et al.; Wu et al.
FeMn / SiMn	Strong wetting/interfacial-composition effects	Interface-controlled drainage/adhesion	Do not transfer steel interfacial data directly to ferroalloys	Bao et al.; Bublik et al.
Pb/Zn / complex slags	Subliquidus solids and variable reduction chemistry	Suspension rheology + generation of collector phase	Treat apparent viscosity and solid fraction explicitly	Vergote et al.; Rämä et al.; Tian et al.
Ni/Co/PGM / secondary feeds	Collector formation and multiphase chemistry	Reaction-generated droplets + capture/settling	Close metal balance across collector, slag, and volatile paths	Ruismäki et al.; Gu et al.; Heo et al.; Tsebe & Steenkamp

Note. Adapted from the metal-specific evidence synthesized in this review. The table is intentionally qualitative because direct numerical comparison across slag families is not physically justified without harmonized property and scale data.

The comparison in Table 6 answers RQ4: mechanisms are transferable at the level of force balances and sequence—generation, collision, film drainage, growth, and separation—but property values and even the sign of a compositional effect are not universally transferable. Transfer therefore requires re-estimation of interfacial properties, rheology, phase state, and hydrodynamic regime for the specific metal–slag pair.

MODELING, VISUALIZATION, AND EXPERIMENTAL METHODS

High-temperature visualization and post-mortem characterization

Direct observation is difficult because the systems are opaque, hot, reactive, and often electrically conductive. Sessile-drop and X-ray methods offer controlled access to wetting and interfacial motion, while quenching followed by SEM/EDS, automated mineralogy, or related microscopy can reconstruct droplet-size distributions and interfacial products. In-situ microscale observations of FeO_x–SiO_2 reactions and Al–calcium-silicate interfaces show the mechanistic value of resolving transient interfaces rather than relying only on final slag chemistry (Goto et al., 2024; Matsushita et al., 2021; Minami et al., 2023; Philipson et al., 2024).

Post-mortem methods are powerful but can introduce sampling and solidification bias: droplets may move, coarsen, oxidize, or fragment during cooling. Industrial copper-slag work partly overcomes this by combining automated droplet-size characterization with matrix analysis and recovery data, providing a multi-scale evidence chain (Isaksson et al., 2023).

Physical models and liquid analogs

Room-temperature liquid–liquid and water models isolate hydrodynamic mechanisms with excellent optical access. They are valuable for bubble-interface crossing, droplet sedimentation, and bouncing/coalescence regimes, but similarity requires careful matching of the relevant dimensionless groups. A water model that matches geometry but not viscosity ratio, interfacial tension, density ratio, or Weber/Eötvös regimes can reproduce flow patterns while misrepresenting droplet breakup or coalescence (Cheng et al., 2024; Kumar et al., 2020; McGuan et al., 2022; Morales et al., 2020; Qian et al., 2023; R. Wang, Zhang, et al., 2025).

CFD, interface-resolved, particle, and population-balance models

The supplied literature spans particle methods, smoothed particle hydrodynamics, VOF/interface-resolved calculations, Euler–Lagrange approaches, and droplet residence-time or size-distribution models. These methods

increasingly resolve multiphase flow and interfacial deformation, but most still simplify at least one of the following: dynamic interfacial tension, chemical reaction, breakup/coalescence kernels, evolving slag rheology, or industrial-scale residence-time distribution (Dong et al., 2020; Li et al., 2024; Li & Pistorius, 2021; Mitas et al., 2022; Mitas et al., 2023; Natsui et al., 2020; Schubert et al., 2022; Wan et al., 2024); Q.-M. Wang, Huang, et al., 2023; Wei et al., 2026; Xin et al., 2025; Zhang et al., 2026).

The critical validation target should therefore move beyond matching bulk velocity or temperature. A minimum validation set for a predictive slag-cleaning model should simultaneously include (i) droplet-size distribution before and after the modeled zone, (ii) phase holdup or dispersed-metal inventory, (iii) settling/disengagement time or residence-time distribution, (iv) the slag rheological/liquid-fraction state used by the model, and (v) final metal partitioning in a closed mass balance. Where interfacial chemistry is central, dynamic interfacial tension, wetting, or a validated proxy should also be reported. Without this multi-response validation, a model can be numerically accurate for flow while remaining unreliable for recovery.

Toward digital twins and data-assisted models

The current corpus contains the physical foundations needed for digital-twin development—thermochemical calculations, rheology, CFD, interfacial models, droplet-size/residence-time models, and industrial recovery observations—but few studies close all of them in one continuously updated representation. The near-term opportunity is not a black-box "AI coalescence model"; it is a hybrid model that assimilates measurable plant variables and updates physically meaningful latent states such as viscosity, liquid fraction, droplet-size distribution, and settling capacity (Biswas et al., 2025; Fang et al., 2025; Li et al., 2024; Mitas et al., 2023; J. Wang, Fan, et al., 2025; Q.-M. Wang, Huang, et al., 2023; Wei et al., 2026; Zhang et al., 2026).

Table 7 summarizes the method hierarchy and the principal quantity each method can validate.

Table 7. Experimental and numerical methods for metal-droplet coalescence research

Method	Primary observable	Strength	Main limitation for industrial transfer
Sessile-drop / wetting tests	Contact angle, interface motion, reaction layer	High mechanistic control	Small scale; wall/substrate effects; limited turbulent realism
X-ray / radiographic visualization	Opaque-phase motion, interface, droplet shape	Direct high-temperature observation	Equipment complexity; restricted field of view
Quench + microscopy / automated mineralogy	Droplet size, morphology, interfacial phases	Applicable to real industrial samples	Sampling/solidification bias; not continuous
Room-temperature physical model	Flow, bubble path, collision/rebound	Excellent optical access and repeatability	Similarity constraints; chemistry absent
VOF / interface-resolved CFD	Interface shape, waves, bubble/droplet deformation	Detailed multiphase hydrodynamics	High computational cost; uncertain coalescence/contact models
Euler–Lagrange / particle methods	Large droplet populations and trajectories	Efficient for reactor-scale transport	Sub-grid collision and breakup closures dominate accuracy
Population balance	Size distribution evolution	Directly represents growth/breakup/removal	Requires reliable kernels and source terms
Hybrid / digital-twin concept	Online state + predicted recovery	Potential plant decision support	Needs validated property models, sensors, and closed mass balances

Note. Adapted from Dong et al. (2020), Morales et al. (2020), Li and Pistorius (2021), Natsui et al. (2020), Mitas et al. (2022, 2023), Wang et al. (2023), and Fang et al. (2025).

The table shows that no single method resolves all relevant scales. The strongest studies combine mechanistic observations, property measurements, and a reactor-scale outcome rather than relying on a single technique in isolation.

INDUSTRIAL RECOVERY STRATEGIES, SCALE-UP, AND RESEARCH GAPS

Controlled settling and slag holding

Controlled holding is the simplest way to exploit coalescence once the slag is sufficiently fluid and droplets have reached a separable size. Industrial copper settling-furnace studies provide direct support for this strategy, but they also show that holding alone cannot compensate for an unfavorable viscosity or size distribution. The practical sequence is therefore slag conditioning → droplet growth → low-turbulence residence → tapping (Isaksson et al., 2023; Isaksson et al., 2021).

Mixing followed by quiescence

Where reduction or interfacial cleaning is kinetically limited, a staged sequence can be preferable: an active stage for reaction and collision followed by a quiet stage for separation. Mechanical-stirring and gas-stirred studies support this logic, while reactor modifications such as internal baffles illustrate a more general strategy of shaping turbulence spatially rather than simply increasing or decreasing total mixing power (He et al., 2020; Morales et al., 2020; Wan et al., 2024; Zhang et al., 2026).

Flux-assisted, rotary, and supergravity recovery

Flux-assisted aluminum recovery uses chemistry to improve contact and oxide-film disruption; rotary operation supplies mixing and heat transfer; and supergravity adds an external separation force that can shorten the time required for disengagement. Recent aluminum and copper studies show the growing emphasis on integrated intensified separation, including salt reuse and online or continuous concepts (Lan et al., 2026; Milani & Timelli, 2023; Milani et al., 2023; Sun et al., 2024; Sun et al., 2025; Z. Wang, Gao, et al., 2023; Wang et al., 2024; Z. Wang, Gao, et al., 2025; Xu et al., 2025).

Supergravity is especially informative mechanistically because it tests whether residual metal is transport-limited. The cited copper-matte study reported 96.79% Cu recovery into the matte phase and reduced average Cu in the slag below 0.11 wt%, demonstrating that stronger body force can overcome slow gravitational separation under suitable chemistry. This should not be interpreted as a universal replacement for slag conditioning; high apparent viscosity, solids, or strong interfacial adhesion can still limit phase migration (Z. Wang, Gao, et al., 2025).

Scale-up criteria

Scale-up should preserve the competition among collision, breakup, and separation, not just geometric similarity. At minimum, pilot and industrial studies should report slag composition and temperature, liquid fraction or rheological state, droplet-size distribution before and after the intervention, mixing or gas-flow intensity, a transferable hydrodynamic metric where possible (e.g., power density or relevant dimensionless groups), residence/holding time, total and matrix metal content, recovered-metal quality, uncertainty bounds, and a closed mass balance. Large-scale side-blown and industrial recycling studies show that geometry and local turbulence can materially alter bubble and interface behavior (Fang et al., 2025; Pichat et al., 2020; Wan et al., 2024).

Critical knowledge gaps

Ten gaps recur across the evidence base. First, industrial droplet-size distributions are rarely measured before and after process changes. Second, in-situ high-temperature observations remain scarce. Third, dynamic interfacial tension is often replaced by a constant. Fourth, subliquidus rheology and solid morphology are underreported. Fifth, metal balances often do not separate dissolved from entrained metal. Sixth, mixing intensity is described by equipment settings rather than comparable hydrodynamic metrics. Seventh, population-balance kernels are weakly validated. Eighth, pilot-scale experiments with uncertainty bounds are limited. Ninth, recovery is seldom linked to recovered-metal quality and downstream slag value. Tenth, economic and environmental trade-offs of

additives or intensified-force methods are rarely integrated into the same optimization (Isaksson et al., 2023; Klaffenbach et al., 2023; Li et al., 2024; Mitas et al., 2023; Vergote et al., 2025; Q.-M. Wang, Huang, et al., 2023; Z. Wang, Gao, et al., 2025; Zhang et al., 2026).

Proposed D–I–S–H–R framework

The proposed framework treats recovery as the output of five coupled state descriptions: Droplet, Interface, Slag, Hydrodynamics, and Recovery. “Droplet” defines the source and size distribution; “Interface” defines wetting, dynamic interfacial tension, films, and reaction; “Slag” defines viscosity/rheology, density, liquidus, solids, and chemistry; “Hydrodynamics” defines the collision and breakup environment plus residence time; and “Recovery” defines the available settling or forced-separation mechanism and the quality/mass balance of the collected metal.

Figure 7 is inserted here as the central authorial synthesis of the review.

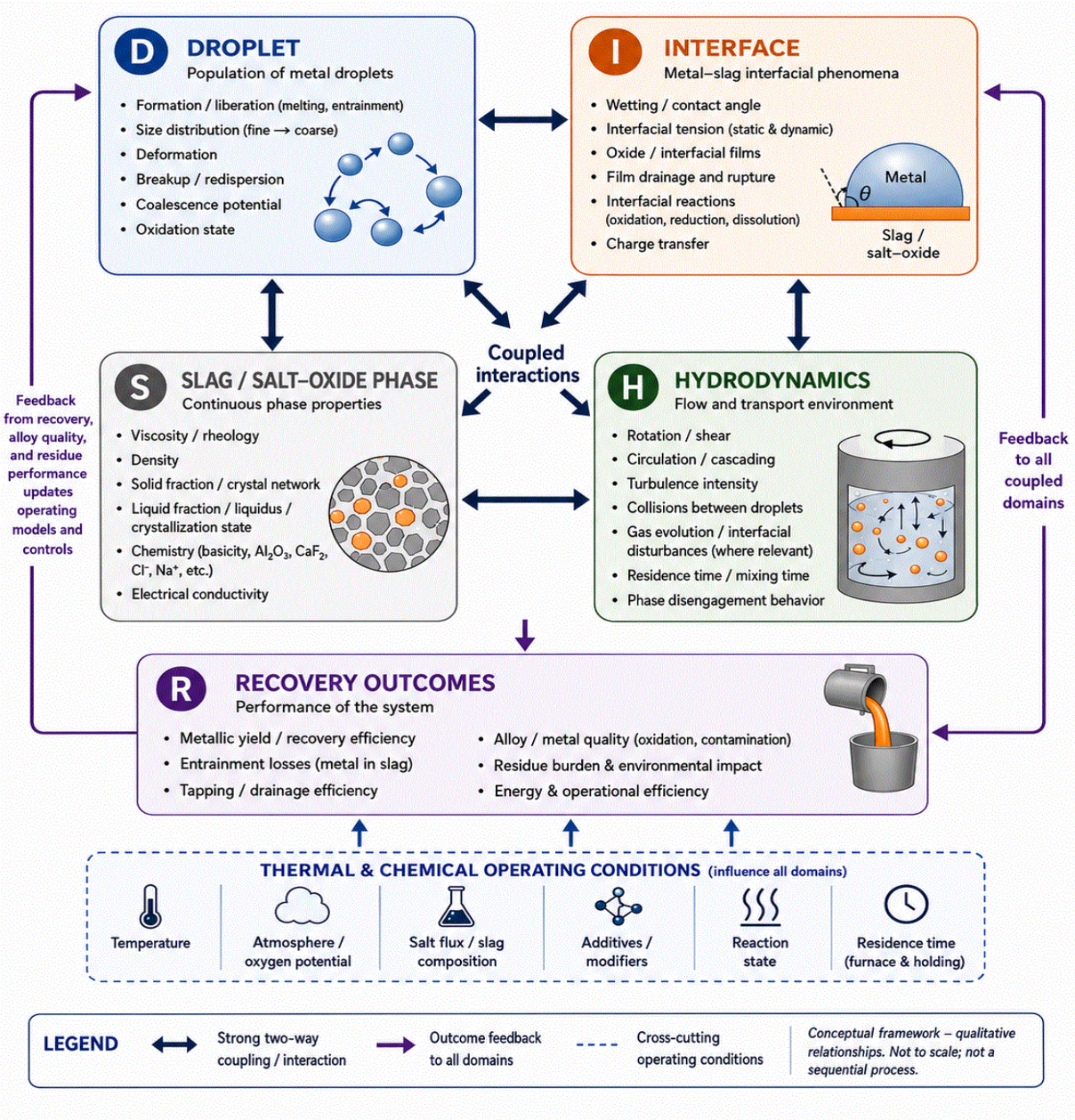

Figure 7. Droplet–Interface–Slag–Hydrodynamics–Recovery (D–I–S–H–R) framework linking mechanism to process outcome.

Note. Author-developed synthesis adapted from the mechanistic evidence reviewed in Sections 3–11, particularly He et al. (2020), Bublik et al. (2021, 2022), McGuan et al. (2022), Isaksson et al. (2023), Qian et al. (2023), Q.-M. Wang, Huang, et al. (2023), and Lai et al. (2026).

ISSN No. 2454-6186 | DOI: 10.47772/IJRISS | Volume X Issue VII July 2026

The feedback arrow is essential. For plant use, each D–I–S–H–R domain should be tied to a measurable state or validated proxy: D to droplet-size distribution and entrainment source; I to wetting, dynamic interfacial behavior, reaction films, or interfacial proxies; S to temperature, composition, liquid fraction, viscosity/apparent rheology, and solids; H to mixing/gas-flow intensity, residence-time history, and collision/breakup regime; and R to separated metal mass, residual entrained versus matrix metal, recovered-metal quality, and a closed balance. Post-heat or post-campaign recovery data should then update the inferred droplet-size and slag-state model rather than being treated only as a final KPI. This makes the framework suitable for future hybrid digital twins and adaptive process control.

Evidence maturity and decision framework

The literature is not uniformly mature. High-temperature interfacial studies have strong mechanistic content but limited plant-scale evidence; copper slag conditioning has genuine industrial evidence; and supergravity has advanced from laboratory concepts toward scale-up demonstrations but remains less established in routine plant practice. Figure 8 separates the strength of scientific evidence from technology-transfer maturity.

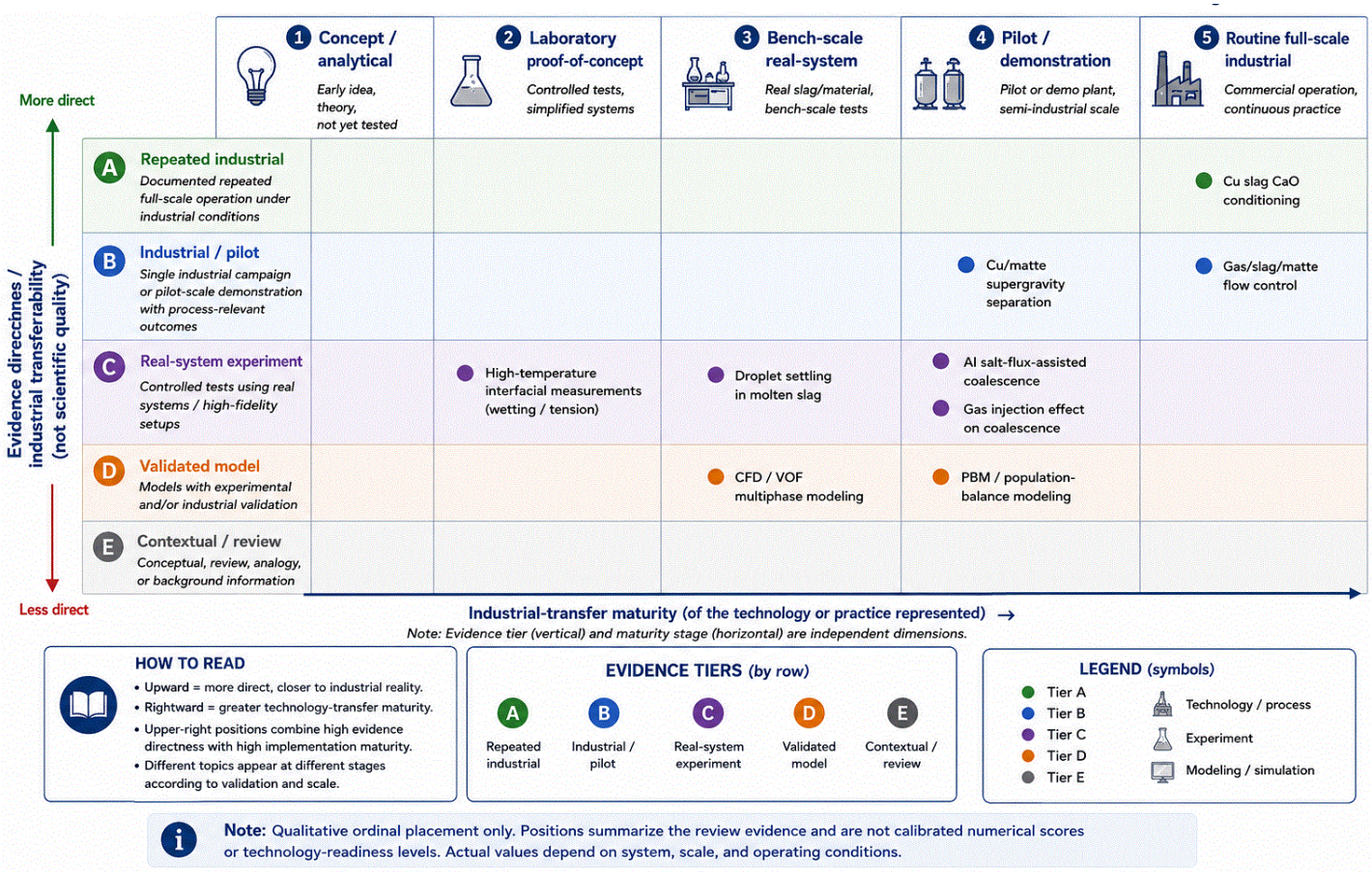

Figure 8. Qualitative matrix of evidence strength and industrial-transfer maturity for representative coalescence and separation approaches.

Note. Author-developed synthesis based on the evidence tiers used in this review and representative studies by Isaksson et al. (2023), Milani et al. (2023), Z. Wang, Gao, et al. (2025), Fang et al. (2025), and Lan et al. (2026). The x-axis uses ordinal implementation classes (concept, laboratory, bench/pilot, demonstration, routine industrial); positions are qualitative and are not calibrated scores.

Figure 8 argues against equating novelty with readiness. A mechanism can be convincingly demonstrated yet remain far from industrial deployment, while a plant intervention can be effective even before every interface-level mechanism is fully resolved. The y-coordinate corresponds to the strongest evidence tier supporting the representative approach, whereas the x-coordinate represents the broadest demonstrated implementation scale in the retained evidence. The matrix is therefore a transparent ordinal synthesis, not a quantitative ranking of technical or economic performance.

Figure 9 converts the D–I–S–H–R framework into a diagnostic sequence. Its first gate prevents a common category error: trying to solve chemical dissolution with a physical coalescence strategy.

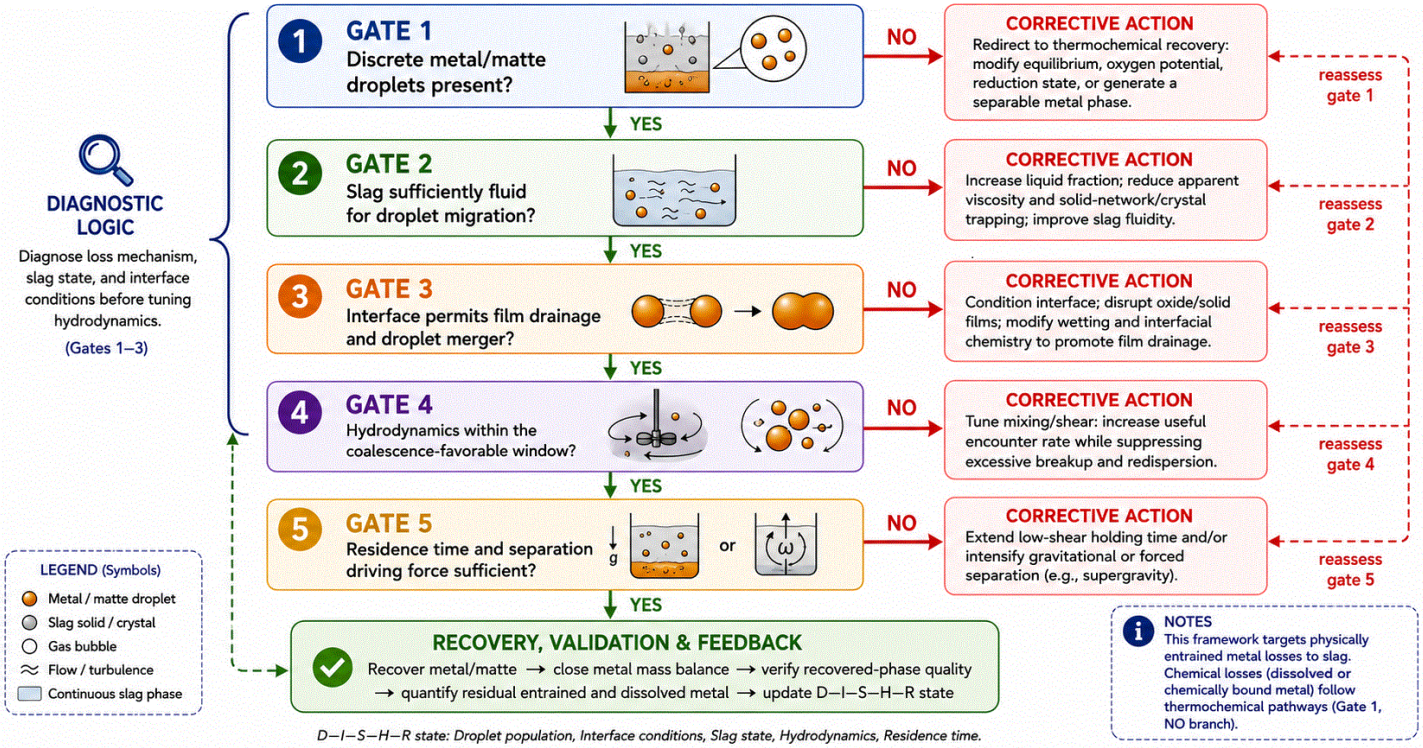

Figure 9. Five-gate decision framework for diagnosing and reducing entrained-metal losses in metallurgical slags.

Note. Author-developed synthesis adapted from the slag-conditioning, interfacial, hydrodynamic, and forced-separation evidence reviewed in this article, including Isaksson et al. (2023), Milani et al. (2023), Fang et al. (2025), Z. Wang, Gao, et al. (2025), and Zhang et al. (2026).

The processes in Figure 9 are as important as the forward path. If residual metal is not present as a discrete droplet phase, equilibrium or reduction chemistry must be altered before physical coalescence can help. If the slag is partially solid or strongly yield-stress dominated, interface tuning or additional mixing is premature. If interfacial films dominate, chemistry and film management become the next lever. Hydrodynamics is adjusted only after these prerequisites are satisfied; if droplets are already large but still retained, the separation force or the available holding time becomes dominant. This gate logic is the proposed practical answer to RQ5.

CONCLUSIONS

This critical review supports five conclusions. First, physically entrained and chemically dissolved metal are fundamentally distinct loss mechanisms and must be diagnosed separately before selecting a recovery strategy. Second, droplet growth is governed by a coupled interface–slag–hydrodynamics problem: collision frequency alone does not determine coalescence because film drainage, interfacial films, dynamic interfacial tension, slag rheology, and contact time intervene between encounter and merger. Third, lower viscosity generally promotes mobility and settling, but it is not an independent optimization target; composition, liquidus, solid fraction, redox state, and interfacial chemistry can change simultaneously. Fourth, greater agitation is not equivalent to greater recovery. Useful operation occupies a finite hydrodynamic window in which collision enhancement exceeds breakup and is followed by sufficient low-turbulence or forced-separation time for enlarged droplets to disengage. Fifth, the main scientific-to-industrial gap is the lack of quantitatively validated links among droplet-size distribution, dynamic interfacial state, non-Newtonian slag behavior, reactor hydrodynamics, and closed metal balances under plant conditions.

The proposed D–I–S–H–R framework addresses this gap by sequencing diagnosis and intervention: identify whether the loss is entrained or dissolved; establish a sufficiently mobile slag; manage oxide/solid films and reactive interfaces; tune mixing to increase useful encounters without creating a finer emulsion; and finally

provide adequate gravitational or forced separation before tapping or solidification. Confidence is not uniform across these steps: the strongest direct industrial anchor in the retained evidence is copper-slag conditioning and settling, high-temperature interfacial studies provide strong mechanism-level evidence but more limited plant transfer, and supergravity represents an emerging intensified-separation route whose scale-up and integration remain less mature. Future studies should therefore report not only residual metal, but also evolving droplet-size distribution, slag rheology and liquid fraction, dynamic interfacial behavior, residence-time history, uncertainty, recovered-metal quality, and a closed mass balance. Such data are required to move coalescence science from isolated high-temperature mechanisms to predictive, validated, and economically meaningful industrial slag-cleaning strategies.

DECLARATIONS

Author contributions: Antonio Clareti Pereira: Conceptualization, methodology, critical analysis, writing—original draft, writing—review and editing.

Funding: This research received no external funding.

Institutional review board statement: Not applicable.

Informed consent statement: Not applicable.

Conflicts of interest: The author declares no conflict of interest.

REFERENCES

1. Avarmaa, K., Klemettinen, L., Michallik, R. M., & Lindberg, D. (2025). Solubility of gold in FeO_x–SiO_2–Al_2O_3 slags at 1300 °C. Mineral Processing and Extractive Metallurgy Review, 46(8), 858–864.
2. Bao, S., Tangstad, M., Tang, K., Einarsrud, K. E., Syvertsen, M., Onsøien, M. I., Kudyba, A., & Bublik, S. (2021). Investigation of two immiscible liquids wetting at elevated temperature: Interaction between liquid FeMn alloy and liquid slag. Metallurgical and Materials Transactions B, 52, 2847–2858.
3. Biswas, J., Gu, K., & Coley, K. S. (2021). Decarburization of bloated droplets: An experimental study to understand the kinetics of decarburization of metallic iron droplets in FeO-containing CaO–SiO_2 slags. Metallurgical and Materials Transactions B, 52(6), 4215–4229.
4. Biswas, J., Gu, K., & Coley, K. S. (2022). Consideration of the competitive adsorption of oxygen and sulfur on the decarburization kinetics of Fe–C droplets in oxidizing slag. Metallurgical and Materials Transactions B, 53(6), 4087–4104.
5. Biswas, J., Hazaveh, P. K., & Coley, K. S. (2025). Slag electrical conductivity and its effect on mass transport and interfacial reaction kinetics. Steel Research International, 96(4), Article 2300701.
6. Bublik, S., Bao, S., Tangstad, M., & Einarsrud, K. E. (2021). Interfacial behaviour in ferroalloys: The influence of sulfur in FeMn and SiMn systems. Metallurgical and Materials Transactions B, 52, 3624–3645.
7. Bublik, S., Tangstad, M., & Einarsrud, K. E. (2022). Interfacial behaviour in ferroalloys: The influence of FeMn slag composition. Metallurgical and Materials Transactions B, 53(5), 3276–3291.
8. Çapkın, İ. Y., & Gökelma, M. (2023). An investigation on inclusions forming during remelting of aluminum and magnesium scraps under a salt flux. JOM, 75(10), 4269–4274.
9. Chang, S., Zou, Z., Liu, J., Isac, M., Cao, X. E., Su, X., & Guthrie, R. I. L. (2021). Study on the slag-metal interfacial behavior under the impact of bubbles in different sizes. Powder Technology, 387, 125–135.
10. Cheng, X., Qing, G., Zhao, Z., & Zhao, B. (2024). Fluid dynamics studies on bottom liquid detachment from a rising bubble crossing a liquid–liquid interface. Metals, 14(9), Article 1005. https://doi.org/10.3390/met14091005
11. Chi, X., Liu, H., Xia, J., Chen, H., Yu, X., Weng, W., & Zhong, S. (2024). Breaking the Fe_3O_4-wrapped copper microstructure to enhance copper–slag separation. International Journal of Minerals, Metallurgy and Materials, 31(10), 2312–2325. https://doi.org/10.1007/s12613-024-2861-4

12. Clift, R., Grace, J. R., & Weber, M. E. (1978). Bubbles, drops, and particles. Academic Press. ISBN 978-0-12-176950-5. No DOI was assigned to the original 1978 edition; the verified bibliographic record lists 380 pages and Academic Press as publisher. Google Books bibliographic record
13. Coulaloglou, C. A., & Tavlarides, L. L. (1977). Description of interaction processes in agitated liquid–liquid dispersions. Chemical Engineering Science, 32(11), 1289–1297. https://doi.org/10.1016/0009-2509(77)85023-9
14. Dong, C., Guo, K., Cai, Q., Chen, R., Tian, W., Qiu, S., & Su, G. H. (2020). Simulation on mass transfer at immiscible liquid interface entrained by single bubble using particle method. Nuclear Engineering and Technology, 52(6), 1172–1179. https://doi.org/10.1016/j.net.2019.11.023
15. Eguchi, T., Nishioka, N., & Takebe, H. (2023). Additive effect of Al_2O_3, CaO, and MgO on the viscosity of FeO_x–SiO_2 slag melt (x = 1.0–1.5). Journal of Sustainable Metallurgy, 9(4), 1487–1498. https://doi.org/10.1007/s40831-023-00741-x
16. Eray, S., Keskinkılıç, E., Topkaya, Y. A., & Geveci, A. (2022). Recovery of iron from Turkish and Iranian red muds. JOM, 74(2), 456–464. https://doi.org/10.1007/s11837-021-05076-0
17. Fang, W., Wan, Z., Hu, Z., Wang, Y., Shi, P., Huang, J., Zhong, L., & Li, M. (2025). Gas–slag–matte multiphase flow and bubble dynamics in an industrial side-blown smelting furnace. Physics of Fluids, 37(8), Article 083356. https://doi.org/10.1063/5.0284052
18. Goto, Y., Kawanishi, S., Natsui, S., Takahashi, J.-I., & Nogami, H. (2024). In situ microscale observation of FeO_x–SiO_2 interfacial reaction. Metallurgical and Materials Transactions B, 55(3), 1735–1753. https://doi.org/10.1007/s11663-024-03063-9
19. Gu, H., Tan, C., Yu, Y., Jiang, W., Wang, H., Hu, J., & Wang, H. (2025). Co-treatment of spent catalyst leaching residue with low-grade Pt/Pd and copper slag to recover valuable metals. Separation and Purification Technology, 375, Article 133792. https://doi.org/10.1016/j.seppur.2025.133792
20. He, M., Wang, N., Hou, Q., Chen, M., & Yu, H. (2020). Coalescence and sedimentation of liquid iron droplets during smelting reduction of converter slag with mechanical stirring. Powder Technology, 362, 550–558. https://doi.org/10.1016/j.powtec.2019.12.020
21. Heo, J., Park, J., & Park, J. H. (2022). Effect of pyro-processing conditions on impurity removal and precious metal enrichment in waste printed circuit board (WPCB) recycling process. Resources, Conservation and Recycling, 179, Article 106068. https://doi.org/10.1016/j.resconrec.2021.106068
22. Hinze, J. O. (1955). Fundamentals of the hydrodynamic mechanism of splitting in dispersion processes. AIChE Journal, 1(3), 289–295. https://doi.org/10.1002/aic.690010303
23. Hu, M., Zhu, D., Pan, J., Guo, Z., Yang, C., Li, S., & Cao, W. (2025). Fe–P alloy production from high-phosphorus oolitic iron ore via efficient pre-reduction and smelting separation. Minerals, 15(8), Article 778. https://doi.org/10.3390/min15080778 .
24. Isaksson, J., Andersson, A., Vikström, T., Lennartsson, A., & Samuelsson, C. (2023). Improved settling mechanisms of an industrial copper smelting slag by CaO modification. Journal of Sustainable Metallurgy, 9(3), 1378–1389. DOI: 10.1007/s40831-023-00733-x. DOI 10.1007/s40831-023-00733-x
25. Isaksson, J., Vikström, T., Lennartsson, A., & Samuelsson, C. (2021). Influence of process parameters on copper content in reduced iron silicate slag in a settling furnace. Metals, 11(6), Article 992. DOI: 10.3390/met11060992.
DOI 10.3390/met11060992
26. Jing, B., Tan, J., Li, Q., & Liang, C. (2025). Liquid phase fraction effect on metal recovery during semi-molten low temperature reduction of pickling sludge. Journal of Sustainable Metallurgy, 11(4), 4575–4584. DOI: 10.1007/s40831-025-01282-1. DOI 10.1007/s40831-025-01282-1
27. Klaffenbach, E., Montenegro, V., Guo, M., & Blanpain, B. (2023). Sustainable and comprehensive utilization of copper slag: A review and critical analysis. Journal of Sustainable Metallurgy, 9(2), 468–496. DOI: 10.1007/s40831-023-00683-4. DOI 10.1007/s40831-023-00683-4
28. Klaffenbach, E., Mostaghel, S., Guo, M., & Blanpain, B. (2021). Thermodynamic analysis of copper smelting, considering the impact of minor elements behavior on slag application options and Cu recovery. Journal of Sustainable Metallurgy, 7(2), 664–683. DOI: 10.1007/s40831-021-00354-2. DOI 10.1007/s40831-021-00354-2

29. Kleeberg, C. (2022). Review on operation of spinel-containing slags of the non-ferrous metallurgy. Materials Science and Technology, 38(10), 607–621. DOI: 10.1080/02670836.2022.2062812. DOI 10.1080/02670836.2022.2062812
30. Kumar, P., & Safarian, J. (2025). Effect of pre-reduction of manganese ore by hydrogen on its smelting behavior and interaction with stable oxides. Journal of Sustainable Metallurgy, 11(3), 2980–3000. DOI: 10.1007/s40831-025-01162-8.
DOI 10.1007/s40831-025-01162-8
31. Kumar, R., Rohilla, L., & Das, A. K. (2020). Passage of a Taylor bubble through a stratified liquid–liquid interface. Industrial & Engineering Chemistry Research, 59(9), 3757–3771. DOI: 10.1021/acs.iecr.9b04235.
DOI 10.1021/acs.iecr.9b04235
32. Lai, C., Jing, B., Tan, J., & Li, Q. (2026). Investigation of iron droplets assembling in molten slag. Colloids and Surfaces A: Physicochemical and Engineering Aspects, 735, Article 139463. DOI: 10.1016/j.colsurfa.2026.139463.
DOI 10.1016/j.colsurfa.2026.139463
33. Lan, X., Gao, J., Feng, G., Li, X., & Guo, Z. (2026). Innovative integration of superimposed extrusion with supergravity for enhanced metallic aluminum recovery from hot dross. Journal of Materials Research and Technology, 41, 2070–2080. DOI: 10.1016/j.jmrt.2026.01.141. DOI 10.1016/j.jmrt.2026.01.141.
34. Li, M., Li, L., Shao, L., Li, W., & Zou, Z. (2024). Influence of solutal Marangoni effect on droplet behavior in metal–slag emulsion system: A numerical study. JOM, 76(11), 6433–6445. https://doi.org/10.1007/s11837-024-06575-6
35. Li, Q., & Pistorius, P. C. (2021). Interface-resolved simulation of bubbles–metal–slag multiphase system in a gas-stirred ladle. Metallurgical and Materials Transactions B, 52(3), 1532–1549. https://doi.org/10.1007/s11663-021-02121-w
36. Li, Z., Li, J., Spooner, S., & Seetharaman, S. (2022). Basic oxygen steelmaking slag: Formation, reaction, and energy and material recovery. Steel Research International, 93(3), Article 2100167. https://doi.org/10.1002/srin.202100167
37. Lin, Y., Yan, B., Shu, Q., & Fabritius, T. (2021). Synergetic valorization of basic oxygen furnace slag and stone coal: Metal recovery and preparation of glass-ceramics. Waste Management, 135, 158–166. https://doi.org/10.1016/j.wasman.2021.08.044
38. Liu, C., Yao, S., Yang, X., Tang, C., & Xing, P. (2026). A novel process for preparing ferrosilicon alloy from coal gasification coarse slag. Silicon, 18(3–4), 1193–1206. https://doi.org/10.1007/s12633-025-03593-0
39. Liu, Y., Cheng, S., & Liu, T. (2023). Effects of entrained slag droplets on slag–metal interface in a gas-stirred ladle. ISIJ International, 63(6), 1017–1024. https://doi.org/10.2355/isijinternational.ISIJINT-2022-164
40. Liu, Y., Cheng, S., & Liu, T. (2024). Study of inclusions-removal and slag–metal dispersion phenomenon in gas-stirred ladle. International Journal of Chemical Reactor Engineering, 22(7), 843–853. https://doi.org/10.1515/ijcre-2024-0090
41. Liu, Y., Xu, L., & Chen, M. (2023). Green and efficient recovery of valuable metals from waste copper slag via co-modification with CaO and Na_2O. Process Safety and Environmental Protection, 180, 959–971. https://doi.org/10.1016/j.psep.2023.10.061
42. Madej, P. (2025). Influence of the reduction rate of slag from oxidation process of Cu–Fe–Pb alloy during reduction (de-coppering) on its viscosity. Metallurgical and Materials Transactions B, 56, 833–851. https://doi.org/10.1007/s11663-024-03381-y.
43. Makhambetov, Y., Kabylkanov, S., Abdulina, S., Zhakan, A., Burumbayev, A., Sadyk, Z., Akhmetov, A., & Sarkar, A. (2026). Sustainable production of chromium–manganese ligatures from low-grade iron–manganese ore and ferrosilicochrome dust: Thermodynamic modeling and experimental verification. Metals, 16(2), Article 184. https://doi.org/10.3390/met16020184
44. Martín Treceño, S., Allanore, A., Bishop, C. M., Marshall, A. T., & Watson, M. (2021). Implications of direct use of slag from ironmaking processes as molten oxide electrolyte. JOM, 73(6), 1899–1908. https://doi.org/10.1007/s11837-021-04681-3

45. Matsushita, T., Belov, I., Siafakas, D., Jarfors, A. E. W., & Watanabe, M. (2021). Interfacial phenomena between molten iron and molten slag–Effect of nitrogen on the Marangoni convection. Journal of Materials Science, 56, 7811–7822. https://doi.org/10.1007/s10853-020-05730-z
46. McGuan, R., Candler, R., & Kavehpour, H. P. (2022). The dynamics of bouncing, partially coalescing, liquid metal droplets in a viscous medium. Journal of Fluid Mechanics, 933, Article A29. https://doi.org/10.1017/jfm.2021.1090
47. Mendoza, S., Garlick, C., Singh, T., Nusheh, M., Yin, B. H., Honeyands, T., & Bumby, C. W. (2026). Melting behavior of hydrogen-reduced vanadium-bearing titanomagnetite ironsand pellets in a laboratory-scale electrode smelter. Journal of Sustainable Metallurgy, 12(2), 1176–1188. https://doi.org/10.1007/s40831-025-01389-5
48. Milani, V., & Timelli, G. (2023). Solid salt fluxes for molten aluminum processing—A review. Metals, 13(5), Article 832. https://doi.org/10.3390/met13050832
49. Milani, V., Vallejo-Olivares, A., Tranell, G., & Timelli, G. (2023). Influence of cryolite content on the thermal properties and coalescence efficiency of NaCl–KCl salt flux. In S. Broek (Ed.), Light Metals 2023 (pp. 928–935). Springer. https://doi.org/10.1007/978-3-031-22532-1_123
50. Minami, T., Katoh, K., Wakimoto, T., Ueda, Y., & Iguchi, M. (2023). Dynamic behavior of a metal droplet in contact with slag–metal interface. Journal of the Japanese Society for Experimental Mechanics, 23(1), 56–63. https://doi.org/10.11395/jjsem.23.56
51. Mirjalili, S., & Chan, W. H. R. (2021). Linear stability of a thin fluid film interacting with its surrounding bulk fluid. Physics of Fluids, 33(7), Article 072104. https://doi.org/10.1063/5.0056855.
52. Mitas, B., Visuri, V.-V., & Schenk, J. (2022). Mathematical modeling of the ejected droplet size distribution in the vicinity of a gas–liquid impingement zone. Metallurgical and Materials Transactions B, 53(5), 3083–3094. https://doi.org/10.1007/s11663-022-02588-1
53. Mitas, B., Visuri, V.-V., & Schenk, J. (2023). Modeling the residence time of metal droplets in slag during BOF steelmaking. Metallurgical and Materials Transactions B, 54(4), 1938–1953. https://doi.org/10.1007/s11663-023-02808-2
54. Mongoljiibuu, S.-O., Lastam, J., Ditscherlein, R., Ebert, D., Müller, M., & Peuker, U. A. (2025). Chromium in slag from SOEL interconnects remelting: Characterization and recycling potential. Minerals, 15(9), Article 904. https://doi.org/10.3390/min15090904
55. Moosavi-Khoonsari, E., & Mostaghel, S. (2024). Thermodynamic assessment of tin-smelting from cassiterite concentrates. Canadian Metallurgical Quarterly, 63(3), 901–914. https://doi.org/10.1080/00084433.2023.2266209
56. Moosavi-Khoonsari, E., & Tripathi, N. (2024). Gold recovery from smelting copper sulfide concentrate. Processes, 12(12), Article 2795. https://doi.org/10.3390/pr12122795
57. Morales, R. D., Calderón-Hurtado, F. A., Chattopadhyay, K., & Guarneros Guarneros, S. J. (2020). Physical and mathematical modeling of flow structures of liquid steel in ladle stirring operations. Metallurgical and Materials Transactions B, 51(2), 628–648. https://doi.org/10.1007/s11663-019-01759-x
58. Nababan, D. C., Mukhlis, R., Durandet, Y., Prentice, L. H., & Rhamdhani, M. A. (2024a). Separation of Li and Co from $LiCoO_2$ cathode material through aluminothermic reduction: Investigation of the thermite reaction. Metallurgical and Materials Transactions B, 55(2), 905–924. https://doi.org/10.1007/s11663-024-03003-7
59. Nababan, D. C., Mukhlis, R., Durandet, Y., Prentice, L. H., & Rhamdhani, M. A. (2024b). Separation of Li and Co from $LiCoO_2$ cathode material through aluminothermic reduction: Thermodynamic calculations and experimental results. Metallurgical and Materials Transactions B, 55(1), 352–375. https://doi.org/10.1007/s11663-023-02962-7
60. Natsui, S., Tonya, K., Nogami, H., Kikuchi, T., Suzuki, R. O., Ohno, K.-I., Sukenaga, S., Kon, T., Ishihara, S., & Ueda, S. (2020). Numerical study of binary trickle flow of liquid iron and molten slag in coke bed by smoothed particle hydrodynamics. Processes, 8(2), Article 221. https://doi.org/10.3390/pr8020221
61. Page, M. J., McKenzie, J. E., Bossuyt, P. M., Boutron, I., Hoffmann, T. C., Mulrow, C. D., Shamseer, L., Tetzlaff, J. M., Akl, E. A., Brennan, S. E., Chou, R., Glanville, J., Grimshaw, J. M., Hróbjartsson, A., Lalu, M. M., Li, T., Loder, E. W., Mayo-Wilson, E., McDonald, S., … Moher, D. (2021). The PRISMA

2020 statement: An updated guideline for reporting systematic reviews. BMJ, 372, Article n71. https://doi.org/10.1136/bmj.n71

62. Park, W.-B., Park, J., Park, Y.-J., Park, S.-C., & Kang, Y.-B. (2026). Experimental investigation of hydrogen-based DRI melting behavior coupled with thermodynamic prediction for optimization of carburizing agents and flux blending conditions. Metallurgical and Materials Transactions B. Advance online publication. https://doi.org/10.1007/s11663-026-04164-3. .
63. Pelusi, F., Guglietta, F., Sega, M., Aouane, O., & Harting, J. (2023). A sharp interface approach for wetting dynamics of coated droplets and soft particles. Physics of Fluids, 35(8), Article 082126. https://doi.org/10.1063/5.0160096.
64. Pereira, A. C. (2025a). Aluminum scrap recycling for foundry alloys: Review of technological advances and circular economy challenges. Revista DCS, 22(84), Article e3867. https://doi.org/10.54899/dcs.v22i84.3867.
65. Pereira, A. C. (2025b). From can to sheet: A critical review of aluminum can recycling processes, technologies, and sustainability dimensions (2020–2025). Revista FT, 29(151), 19–20. https://doi.org/10.69849/revistaft/pa10202510261019. .
66. Philipson, H. G. R., Wallin, M., & Einarsrud, K. E. (2024). Investigation of liquid–liquid reaction phenomena of aluminum in calcium silicate slag. Materials, 17(7), Article 1466. https://doi.org/10.3390/ma17071466.
67. Pichat, A., Vassel, A., Menet, P. Y., & Jouët-Pastre, L. (2020). Constellium R&D approach in recycling, from lab to industrial scale. In A. Tomsett (Ed.), Light Metals 2020 (pp. 1073–1082). Springer. https://doi.org/10.1007/978-3-030-36408-3_146. O .
68. Prince, M. J., & Blanch, H. W. (1990). Bubble coalescence and break-up in air-sparged bubble columns. AIChE Journal, 36(10), 1485–1499. https://doi.org/10.1002/aic.690361004.
69. Qian, L., He, W., Liu, J., Zhu, C., Zhou, F., Ding, H., & Lin, J. (2023). Experimental investigation of the sedimentation behavior of metal droplets in liquid–liquid systems. Physics of Fluids, 35(2), Article 023304. https://doi.org/10.1063/5.0135636.
70. Rämä, M., Klemettinen, L., Rinne, M., Taskinen, P., Michallik, R. M., Salminen, J., & Jokilaakso, A. (2023). Processing of a zinc leach residue by a non-fossil reductant. ACS Omega, 8(24), 21450–21463. https://doi.org/10.1021/acsomega.3c00250.
71. Romero, J. L., Recksiek, V., Debastiani, R., Hossain, M. N., Blenau, L., Charitos, A., Väisänen, A. O., & Patil, A. B. (2026). Pyrometallurgical valorization of Waelz, fayalite, and Linz–Donawitz slag mixtures. Scientific Reports, 16, Article 9539. https://doi.org/10.1038/s41598-026-44763-3. A
72. Ruismäki, R., Dańczak, A., Klemettinen, L., Taskinen, P., Lindberg, D., & Jokilaakso, A. (2020). Integrated battery scrap recycling and nickel slag cleaning with methane reduction. Minerals, 10(5), Article 435. https://doi.org/10.3390/min10050435
73. Schrama, F. N. H., Beunder, E. M., Panda, S. K., Visser, H.-J., Moosavi-Khoonsari, E., Sietsma, J., Boom, R., & Yang, Y. (2021). Optimal hot metal desulphurisation slag considering iron loss and sulphur removal capacity part I: Fundamentals. Ironmaking & Steelmaking, 48(1), 1–13. https://doi.org/10.1080/03019233.2021.1882647
74. Schubert, C., Eickhoff, M., & Pfeifer, H. (2022). Numerical simulations of the molten metal droplet formation in the electroslag remelting process with a rotating electrode. Steel Research International, 93(12), Article 2100765. https://doi.org/10.1002/srin.202100765
75. Silva, A. M. B., Oliveira, M. A., Peixoto, J. J. M., & da Silva, C. A. (2021). Slag–steel emulsification on a modified RH degasser. Metallurgical and Materials Transactions B, 52(4), 2111–2125. https://doi.org/10.1007/s11663-021-02161-2
76. Spooner, S., Li, Z., & Sridhar, S. (2020). Hidden phenomena during transient reaction trajectories in liquid metals processing. Metallurgical and Materials Transactions B, 51(4), 1301–1314. https://doi.org/10.1007/s11663-020-01880-2
77. Sun, B., Guo, L., Wang, Z., Lan, X., & Guo, Z. (2024). Sustainable recycling of pure aluminum from waste chips under supergravity-enhanced separation: A cleaning process. Sustainable Materials and Technologies, 42, Article e01148. https://doi.org/10.1016/j.susmat.2024.e01148
78. Sun, B., Guo, L., Wang, Z., Lan, X., & Guo, Z. (2025). Direct collection and reuse of dispersed aluminum chips through salt flux and supergravity enrichment: Less salt consumption and circular economy. Journal of Cleaner Production, 521, Article 146230. https://doi.org/10.1016/j.jclepro.2025.146230

79. Suzuki, M., & Nakamoto, M. (2022). Effect of B_2O_3 addition to slag on the dynamic change behavior of interfacial tension between liquid iron and molten slag. ISIJ International, 62(7), 1334–1340. https://doi.org/10.2355/isijinternational.ISIJINT-2021-605
80. Suzuki, M., Iwakura, K., Tsukaguchi, Y., & Mishima, K. (2024). Effect of fluoride ions in slag on the dynamic change of the interfacial tension between liquid iron and molten slag. ISIJ International, 64(15), 2217–2225. https://doi.org/10.2355/isijinternational.ISIJINT-2024-134
81. Tangstad, M., Olsen, J. E., Ringdalen, E., Ksiazek, M., Reynolds, Q., & Steenkamp, J. (2022). Conceptual tapping model of Mn-ferroalloy furnaces. JOM, 74(11), 3962–3970. https://doi.org/10.1007/s11837-022-05474-y.
82. Tian, M., Wang, Q., Wang, S., Wan, X., Wang, Q., & Guo, X. (2024). Multiphase equilibrium relationships between copper matte and CaO–Al_2O_3-bearing iron silicate slags in combined smelting of WEEE and copper concentrates. Sustainability, 16(2), Article 890. DOI: 10.3390/su16020890. DOI / publisher page
83. Tian, X., Guo, Z., Li, B., Zhu, D., Pan, J., Yang, C., Li, S., & Zhao, F. (2026). Green utilization of zinc smelting slag by hydrogen reduction: Role of MgO in metal separation and recovery. Process Safety and Environmental Protection, 212, Article 108918. DOI: 10.1016/j.psep.2026.108918. DOI / publisher page
84. Tsebe, S. P., & Steenkamp, J. D. (2024). Development of an integrated process flowsheet to recover valuable metals from waste cathode ray tubes and printed circuit boards. Journal of Sustainable Metallurgy, 10(1), 224–240. DOI: 10.1007/s40831-023-00775-1. DOI / Springer
85. Vallejo-Olivares, A., Høgåsen, S., Kvithyld, A., & Tranell, G. (2022). Thermal de-coating pre-treatment for loose or compacted aluminum scrap and consequences for salt-flux recycling. Journal of Sustainable Metallurgy, 8(4), 1485–1497. DOI: 10.1007/s40831-022-00612-x. DOI / Springer
86. Vergote, O., Van den Bulck, A., Bellemans, I., & Verbeken, K. (2025). Rheological behavior of slag–melilite suspensions in pyrometallurgical secondary lead smelter systems. Journal of Rheology, 69(6), 973–989. DOI: 10.1122/8.0001033. DOI
87. Wan, B., Li, W., Liu, F., Lu, T., Jin, S., Wang, K., Yi, A., Tian, J., & Chen, W. (2020). Determination of fluoride component in the multifunctional refining flux used for recycling aluminum scrap. Journal of Materials Research and Technology, 9(3), 3447–3459. DOI: 10.1016/j.jmrt.2020.01.082. DOI / Elsevier
88. Wan, Z., Yang, S., & Wang, H. (2024). Multiphase stirring dynamics of gas–slag–matte in large-scale side-blown copper bath smelting process. Journal of Sustainable Metallurgy, 10(2), 992–1006. DOI: 10.1007/s40831-024-00841-2. DOI / Springer
89. Wang, G., Hui, H., Cui, Y., Li, X., Yang, S., Yang, Y., & He, Y. (2026). The interfacial adhesion behaviors of sedimentation zone in flash smelting based on DFT calculation (Part II)—The adhesion mechanisms of Fe_3O_4 with FeS, Ni_3S_2 and Cu_2S. Metallurgical and Materials Transactions B, 57(3), 1605–1619. DOI: 10.1007/s11663-026-03948-x. DOI / Springer
90. Wang, J., Fan, E., & Wu, Y. (2025). Numerical modeling of Marangoni flow between steel droplet and slag induced by concentration gradient. Canadian Metallurgical Quarterly. Advance online publication. DOI: 10.1080/00084433.2025.2580025. DOI / Taylor & Francis
91. Wang, Q.-M., Huang, M.-X., Yan, S.-Y., Wang, S.-S., Tian, Q.-H., & Guo, X.-Y. (2023). Hydrodynamic simulation of metal droplet settlement in molten slag. Transactions of Nonferrous Metals Society of China, 33(4), 1244–1257. DOI: 10.1016/S1003-6326(23)66179-5. DOI
92. Wang, R., Zhang, B., Liu, C., & Jiang, M. (2025). Physical modeling of bottom-blown bubble penetration dynamics at slag/metal interface in metallurgical reactors. Colloids and Surfaces A: Physicochemical and Engineering Aspects, 727, Article 138296. DOI: 10.1016/j.colsurfa.2025.138296. DOI / Elsevie.
93. Wang, Z., Gao, J., Lan, X., & Guo, Z. (2023). Sustainable recovery of metallic Al and reuse of molten salt in Al dross: Salt flux erosion and super-gravity separation. Journal of Cleaner Production, 431, Article 139809. https://doi.org/10.1016/j.jclepro.2023.139809
94. Wang, Z., Gao, J., Lan, X., & Guo, Z. (2024). Joint utilization and harmless elimination of aluminum dross and refined magnesium slag to simultaneously recover metallic aluminum and fusing agent. Journal of Environmental Management, 366, Article 121680. https://doi.org/10.1016/j.jenvman.2024.121680
95. Wang, Z., Gao, J., Lan, X., & Guo, Z. (2025). An eco-friendly approach for enhanced separation and efficient recovery of copper matte from molten copper smelting slag via supergravity. Process Safety and Environmental Protection, 202, Article 107707. https://doi.org/10.1016/j.psep.2025.107707

96. Wei, G., Wang, H., Ju, J., Yang, Y., & Jiang, X. (2026). Kinetic model for vanadium extraction by CO_2–O_2 mixed injection based on interfacial reactions of emulsified droplets. Metallurgical and Materials Transactions B. Advance online publication. https://doi.org/10.1007/s11663-026-04188-9
97. Wu, C., Wang, J., Bai, J., Kong, L., Guo, Z., Li, H., Bai, Z., & Li, W. (2026). Mechanistic insights into metallic iron-induced changes in viscosity, structure, and iron agglomeration of fixed-bed gasifier slag. Fuel, 424, Article 139397. https://doi.org/10.1016/j.fuel.2026.139397
98. Xin, J., Wang, N., Chen, M., & Chen, C. (2020). Slag–metal separation and reduction behaviors of vanadium-bearing titanomagnetite metalized pellets. ISIJ International, 60(5), 823–831. https://doi.org/10.2355/isijinternational.ISIJINT-2019-529
99. Xin, J., Wang, N., Chen, M., & Chen, C. (2021). Direct alloying of molten steel with vanadium slag as a substitute of ferrovanadium: Self-reduction behavior of vanadium slag briquette with aluminum dross addition. Metallurgical and Materials Transactions B, 52(2), 815–829. https://doi.org/10.1007/s11663-020-02055-9
100. Xin, Z.-C., Lin, W.-H., Zhang, J.-S., Peng, K.-X., & Liu, Q. (2025). Modeling the decarburization of expansion droplets based on the solid phase ratio of slag and data fitting during BOF steelmaking process. Scientific Reports, 15, Article 16346. https://doi.org/10.1038/s41598-025-01424-1
101. Xu, K., Wang, Z., Chu, R., Sun, B., Li, J., & Guo, Z. (2025). Recovery of aluminum–zinc alloy from hot-dip aluminum–zinc galvanizing bottom slag by super-gravity separation: An on-line separation and recycling technology. Sustainable Materials and Technologies, 46, Article e01777. https://doi.org/10.1016/j.susmat.2025.e01777
102. Xu, L., Li, X., Liu, Y., Chen, M., & Wang, N. (2023). Recovery of low phosphorus iron from steel slag using secondary aluminum dross as the reductant. Journal of Environmental Chemical Engineering, 11(5), Article 110973. https://doi.org/10.1016/j.jece.2023.110973
103. Xu, L., Liu, Y., Chen, M., & Wang, N. (2022). Efficient recycling of valuable metals from waste copper slag by using secondary aluminum dross as a novel reductant. Metallurgical and Materials Transactions B, 53(5), 2824–2837. https://doi.org/10.1007/s11663-022-02567-6
104. Xu, L., Zhang, D., Liu, Y., & Chen, M. (2022). Iron recovery from waste copper slag by using coal and secondary aluminum dross as co-reductants. JOM, 74(5), 2029–2036. https://doi.org/10.1007/s11837-022-05218-y
105. Xu, X., Zhou, S., Li, B., Wei, Y., & Wang, H. (2025). Investigation interfacial wetting behavior of copper matte/slag/Fe_3O_4 enriched intermediate layer during high temperature smelting. Metallurgical and Materials Transactions B, 56(1), 449–471. https://doi.org/10.1007/s11663-024-03370-1
106. Zhang, J., Zhao, B., & Yan, B. (2023). Analysis of emulsification behavior and kinetics of reaction between high-Al molten steel and CaO–SiO_2 flux. Metallurgical and Materials Transactions B, 54(3), 981–988. https://doi.org/10.1007/s11663-023-02749-w
107. Zhang, L., & Chen, M. (2023). Recovery of valuable metals and production of Fe–V crude alloy from vanadium-enriched slag using aluminum dross as a reductant. JOM, 75(4), 1180–1191. https://doi.org/10.1007/s11837-022-05561-0
108. Zhang, P., Zhang, H., Deng, G., Li, D., Hu, J., Tan, C., Yu, Y., Fan, R., & Wang, H. (2026). Turbulence modulation via internal baffles for intensified slag–matte separation in gas-stirred reactors. Journal of Sustainable Metallurgy, 12(3), 3181–3199. https://doi.org/10.1007/s40831-026-01503-1
109. Zhao, B., Zhang, J., & Yan, B. (2022). Interfacial phenomena and reaction kinetics between high Al molten steel and CaO–SiO_2-type flux. Metals, 12(3), Article 391. https://doi.org/10.3390/met12030391
110. Zhou, H., Huang, C., Wang, F., & Yang, B. (2026). An efficient smelting process for recovering precious metals, copper, and iron from copper converter slag. Journal of Sustainable Metallurgy. Advance online publication. https://doi.org/10.1007/s40831-026-01580-2
111. Zhu, Y., Li, B., Wei, Y., Zhou, S., & Wang, H. (2025). Simultaneous recovery of valuable metals and detoxification of organics through co-smelting of waste printed circuit boards and copper slag. Chemical Engineering Jour*nal, 525*, Article 170032. https://doi.org/10.1016/j.cej.2025.170032